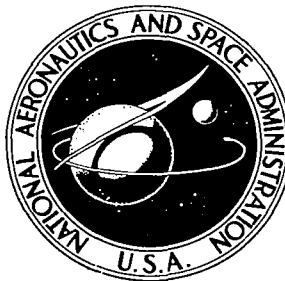


**NASA TECHNICAL
MEMORANDUM**

NASA TM X-2324



NASA TM X-2324

0151980



TECH LIBRARY KAFB, NM

**LOAN COPY: RETURN
AFWL (DOGL)
KIRTLAND AFB, N. M.**

**SERT II SPACECRAFT
ATTITUDE RESPONSE**

*by Bruce E. LeRoy, John D. Regetz,
and Robert R. Lovell*

*Lewis Research Center
Cleveland, Ohio 44135*



0151980

3. Recipient's Catalog No.

1. Report No. NASA TM X-2324		2. Government Accession No.		3. Recipient's Catalog No.	
4. Title and Subtitle SERT II SPACECRAFT ATTITUDE RESPONSE				5. Report Date July 1971	
				6. Performing Organization Code	
7. Author(s) Bruce E. LeRoy, John D. Regetz, and Robert R. Lovell				8. Performing Organization Report No. E-6218	
9. Performing Organization Name and Address Lewis Research Center National Aeronautics and Space Administration Cleveland, Ohio 44135				10. Work Unit No. 120-26	
				11. Contract or Grant No.	
12. Sponsoring Agency Name and Address National Aeronautics and Space Administration Washington, D.C. 20546				13. Type of Report and Period Covered Technical Memorandum	
				14. Sponsoring Agency Code	
15. Supplementary Notes					
16. Abstract <p>This report presents an analysis of the SERT II attitude response. Detailed analyses of magnetic, solar pressure, and ion thruster disturbance torques are presented. The attitude responses indicated by linearized equations of motion and a complete simulation of the satellite are compared to flight data. The discrepancies between flight and predicted data are attributed to errors in the estimation of satellite magnetic moments. The use of magnetic moments derived from the flight data resulted in a good correlation. Thrust vector orientation of the ion engines was a potential problem before the flight, so the capability of gimbaling the ion engines was provided. In flight, however, the misalignments were found to be small and no corrections of the thrust vector orientations were made.</p>					
17. Key Words (Suggested by Author(s)) Attitude control Magnetic moments Control moment gyros Ion thrusters Gravity-gradient				18. Distribution Statement Unclassified - unlimited	
19. Security Classif. (of this report) Unclassified		20. Security Classif. (of this page) Unclassified		21. No. of Pages 66	
				22. Price* \$3.00	

SERT II SPACECRAFT ATTITUDE RESPONSE

by Bruce E. LeRoy, John D. Regetz,
and Robert R. Lovell

Lewis Research Center

SUMMARY

This report presents an analysis of the SERT II attitude response. Detailed analyses of magnetic, solar pressure, and ion thruster disturbance torques are presented. The attitude responses indicated by linearized equations of motion and a complete simulation of the satellite are compared to flight data. The discrepancies between flight and predicted data are attributed to errors in the estimation of satellite magnetic moments. The use of magnetic moments derived from the flight data resulted in a good correlation. Thrust vector orientation of the ion engines was a potential problem before the flight, so the capability of gimbaling the ion engines was provided. In flight, however, the misalignments were found to be small and no corrections of the thrust vector orientations were made.

INTRODUCTION

The SERT II spacecraft (Space Electric Rocket Test) was launched on February 3, 1970, into a near-polar "sun-synchronous" orbit. The primary mission objectives were a 6-month life test of a mercury-bombardment ion thruster system and the determination of the thruster system operating characteristics in a space environment. Power for the experiments and housekeeping was provided by two foldout solar panels, which are rigidly fixed to the body.

The orbiting vehicle consists of an Agena with the solar arrays mounted to the aft equipment rack and the spacecraft and spacecraft support unit mounted to the forward equipment rack. The inertial distribution of this configuration is such that it is gravity-gradient stabilized. The axis of minimum moment of inertia normally aligns with the local vertical, and the axis of maximum moment of inertia aligns with the orbit plane perpendicular. Two control moment gyroscopes (CMG's) are added to provide rate

damping. After orbit injection, the spacecraft is initially oriented by the Agena cold gas attitude control system.

This report presents an analysis of the SERT II attitude response. Preflight estimates of attitude perturbations and the resulting satellite response are compared to actual flight data. Based on the flight data, the satellite magnetic moments are calculated and compared to measurements taken on the ground. The satellite response to ion engine misalignments is also analyzed and estimates of the misalignments obtained.

The report derives in detail the solar pressure, magnetic, and ion thruster misalignment torques. Although gravity-gradient control moment gyro stabilization is not new (refs. 1 to 4), the report derives the satellite equations in a form different from those in the references.

CONFIGURATION AND AXIS SYSTEMS

The orbiting vehicle consists of an Agena with solar arrays mounted to the aft equipment rack and the spacecraft and spacecraft support unit (SSU) mounted to the forward equipment rack. As shown in figure 1, the ion thrusters are mounted to the spacecraft and aligned so that their thrust vectors pass nominally through the vehicle center of mass. Two control moment gyroscopes (CMG's) are mounted in the spacecraft support unit.

Three body-centered axis systems are used in this report. They are the reference axis system, the geometric axis system, and the body (or principal) axis system. The reference axis system is defined as follows: the X_R axis is perpendicular to the earth-satellite radius vector, in the orbit plane, and positive in the direction of the satellite velocity vector; the Y_R axis is perpendicular to the orbit plane and opposite in sense from the orbit angular momentum vector; the Z_R axis is in the orbit plane and opposite in sense from the radius vector. Figure 2 shows the relation between this coordinate system and the earth. The geometric axis system is fixed in the satellite and is defined as follows: the X_G axis is perpendicular to the longitudinal axis of the Agena and parallel to the longest edge of the solar arrays and, when the satellite is properly oriented, is positive in the direction of the orbit velocity; the Y_G axis is perpendicular to the longitudinal axis of the Agena and perpendicular to the plane of the solar arrays; the Z_G axis is along the longitudinal axis of the Agena and is positive in the direction of the spacecraft support unit. Figure 2 also shows the satellite orientation when the two coordinate systems are coincident. The body (or principal) axis system is defined by the principal moments of inertia. The x axis (roll axis) is the axis of intermediate moment of inertia. The y axis (pitch axis) is the axis of maximum moment of inertia, and the z axis (yaw axis) is the axis of minimum moment of inertia. Figure 3 shows that the body and geometric coordinate systems are nearly coincident. Using the com-

puter program described in reference 5, the direction cosine matrix relating the body and geometric systems is found to be

$$\begin{bmatrix} x \\ y \\ z \end{bmatrix} = \begin{bmatrix} 1.000 & -0.0010 & 0.0024 \\ 0.0010 & 1.0000 & 0.0080 \\ -0.0024 & -0.0080 & 1.0000 \end{bmatrix} \begin{bmatrix} X \\ Y \\ Z \end{bmatrix}_G \quad (1)$$

(All symbols are defined in appendix F.)

The principal (or body) coordinate system and the reference system are related by three Euler angles (ψ , θ , ϕ). As shown in figure 4, the yaw angle ψ is a rotation about Z_R , the rotation about y' is a pitch angle θ , and the rotation about x'' is a roll angle ϕ . These three angles are used to define the satellite attitude with respect to the reference coordinate system. The two coordinate systems are related by

$$\begin{bmatrix} x \\ y \\ z \end{bmatrix} = \begin{bmatrix} C\psi C\theta & S\psi C\theta & -S\theta \\ C\psi S\theta S\phi - S\psi C\phi & C\psi C\phi + S\theta S\phi S\psi & C\theta S\phi \\ C\psi S\theta C\phi + S\psi S\phi & S\psi S\theta C\phi - C\psi S\phi & C\theta C\phi \end{bmatrix} \begin{bmatrix} X \\ Y \\ Z \end{bmatrix}_R \quad (2)$$

The orientation of CMG axes with respect to the body axes is shown in figure 5. Electromagnetic torquers are used to maintain the spin reference axes in the "V" configuration $\pm 28^\circ$ from the negative pitch axis.

Table I gives the SERT II vehicle and orbit parameters, and table II gives the CMG parameters.

SATELLITE DISTURBANCE TORQUES

A complete analysis of solar pressure, magnetic, and ion thruster misalignment torques is given in appendix A. For a linearized analysis, we note here the estimated solar pressure and magnetic torques.

Solar Pressure

In appendix A, the solar pressure torque is calculated in two parts. Torque from solar pressure on the solar array is considered separately from the torque due to solar

pressure on the Agena-spacecraft. Under some simplifying assumptions (small Euler angles, coincidence of the geometric and principal axes), it was found that the torque from solar pressure on the Agena-spacecraft was an order of magnitude smaller than the torque due to the solar array. Since the torque from the Agena-spacecraft tends to cancel the torque from the solar array, a "worst case" analysis may be made by considering only the torque from the solar array. In component form, the solar array torque is given below.

The estimated maximum roll torque occurs when the apparent sun declination δ is zero:

$$T_x = -3.40 \times 10^{-4} \text{ N-m} \quad (3)$$

The estimated maximum constant pitch torque occurs when $\delta = 0$ and the yaw angle ψ is ± 0.1 radian:

$$T_y = \pm 2.26 \times 10^{-5} \text{ N-m} \quad (4)$$

The estimated sinusoidal pitch torque of maximum magnitude occurs when $\delta = 30^\circ$ (the maximum apparent declination):

$$T_y = 9.82 \times 10^{-5} \sin \omega_o^* t \quad (5)$$

Magnetics

The estimated magnetic torques are found from the approximated earth field given in appendix A and the estimated satellite dipole given in appendix B.

The approximate earth field in the body axis system given by equation (A31) is

$$\bar{H} = \begin{bmatrix} 0.1965 \cos \omega_o^* t \\ 0.03 \\ 0.3915 \sin \omega_o^* t \end{bmatrix} \text{ oersteds} \quad (6)$$

From appendix B the worst-case satellite dipole moments are

$$\bar{\rho} = \begin{bmatrix} -9.8 \times 10^4 \\ -8.2 \times 10^4 \\ -9.8 \times 10^4 \end{bmatrix} \text{ A-cm}^2$$

Then from equation (A30) the estimated magnetic torque is

$$\bar{T}_B = \begin{bmatrix} -3.21 \times 10^3 \sin \omega_o^* t + 2.94 \times 10^2 \\ 4.29 \times 10^3 \cos \omega_o^* t \\ 1.611 \times 10^3 \cos \omega_o^* t - 2.94 \times 10^2 \end{bmatrix} \text{ dyne-cm} \quad (7a)$$

or

$$\bar{T}_B = \begin{bmatrix} -3.21 \times 10^{-4} \sin \omega_o^* t + 2.94 \times 10^{-5} \\ 4.29 \times 10^{-4} \cos \omega_o^* t \\ 1.61 \times 10^{-4} \cos \omega_o^* t - 2.94 \times 10^{-5} \end{bmatrix} \text{ N-m} \quad (7b)$$

Equations (3), (4), (5), and (7) are used to estimate the satellite attitude response.

SATELLITE ATTITUDE CONTROL TORQUES

A complete analysis of gravity-gradient CMG control is given in appendix C. The linearized control torques in the body (principal) axis system are

Linearized gravity-gradient torques:

$$T_{ggx} = -3(\omega_o^*)^2 (I_{yy} - I_{zz}) \varphi \quad (8a)$$

$$T_{ggy} = -3(\omega_o^*)^2 (I_{xx} - I_{zz}) \theta \quad (8b)$$

$$T_{ggz} = 0 \quad (8c)$$

Linearized Euler cross-coupling torques:

$$T_{ccx} = -(\omega_o^*)^2 (I_{yy} - I_{zz}) \varphi \quad (9a)$$

$$T_{ccy} = 0 \quad (9b)$$

$$T_{ccz} = -(\omega_o^*)^2 (I_{yy} - I_{xx}) \psi \quad (9c)$$

Linearized CMG torques:

$$T_{\text{CMGX}} = -h \left[2\dot{\psi} \cos 28^\circ + 2\omega_o^* \varphi \cos 28^\circ + \omega_o^* \cos 28^\circ (\sigma_1 + \sigma_2) \right] \quad (10a)$$

$$T_{\text{CMGY}} = -\frac{h^2}{c} \sin 28^\circ \left[2\dot{\theta} \sin 28^\circ - \omega_o^* (\sigma_1 - \sigma_2) \cos 28^\circ - 4e \sin 28^\circ \cos \omega_o^* t \right] \quad (10b)$$

$$T_{\text{CMGZ}} = -\frac{h^2}{c} \cos^2 28^\circ \left[\omega_o^* (\sigma_1 + \sigma_2) + 2\dot{\psi} + 2\omega_o^* \varphi \right] + 2h\dot{\varphi} \cos 28^\circ - 2h\omega_o^* \psi \cos 28^\circ \quad (10c)$$

Equations (8) and (9) show that restoring torque exists about all three principal axes. Equation (10) shows that the CMG's directly damp pitch and yaw rates and provide additional restoring torque about the yaw axis. Equation (10a) is misleading as shown for it appears that the CMG's provide restoring torque about the roll axis. A transient restoring torque in roll exists due only to CMG lags. If it were possible to maintain a constant roll offset while holding pitch and yaw offsets to zero, each CMG gimbal angle would attain a steady-state position of $-\varphi$. Thus the second and third terms of the equation cancel. Although roll rates are not damped directly, the roll axis is the axis of intermediate moment of inertia, and roll energy will be cross coupled into the pitch and yaw axes. Thus, complete three-axis control is accomplished with gravity-gradient CMG torques.

SPACECRAFT RESPONSE

Linearized Equations of Motion

Pitch. - Appendix C derives the linearized equations of rotational motion of the SERT II satellite. From equation (C28) we see that only pitch motion is affected by eccentricity. Using the parameters in table I, we find the pitch eccentricity response to be sinusoidal with a zero-to-peak magnitude of

$$|\theta| = 5.04 e \quad \text{for } c = 2.25 \text{ (N)(m)(sec)} \quad (11a)$$

$$|\theta| = 4.16 e \quad \text{for } c = 4.5 \text{ (N)(m)(sec)} \quad (11b)$$

Equations (C28) are also used to find the steady-state pitch response to constant and sinusoidal disturbances. Assuming $e = 0$, the steady-state step torque response is given by

$$\theta_{\text{step}} = \frac{T_y}{3(\omega_o^*)^2(I_{xx} - I_{zz})} = 56.6 T_y \quad (12)$$

where T_y is in newton-meters. The steady-state frequency response magnitude is given by

$$|\theta_{ss}| = 197.8 |T_y| \quad \text{for } c = 2.25 \text{ (N)(m)(sec)} \quad (13a)$$

$$|\theta_{ss}| = 172.7 |T_y| \quad \text{for } c = 4.5 \text{ (N)(m)(sec)} \quad (13b)$$

Roll. - Equations (C29) are used to find the steady-state roll response to step and sinusoidal disturbance. The step response is given by

$$\varphi_{\text{step}} = \frac{T_x}{4(\omega_o^*)^2(I_{yy} - I_{zz})} = 30.2 T_x \quad (14)$$

where T_x is in newton-meters. The steady-state frequency response magnitude is given by

$$|\varphi_{ss}|_{T_x} = 40.3 |T_x| \quad (15)$$

$$|\varphi_{ss}|_{T_z} = -j 40.3 |T_z| \quad (16)$$

where T_x and T_z are in newton-meters.

Equations (15) and (16) show that the roll response to sinusoidal roll torque is 90° out of phase with the roll response to sinusoidal yaw torques.

Yaw. - Equations (C29) are also used to find the steady-state yaw response to step and sinusoidal disturbances. The step response is given by

$$\psi_{\text{step}} = \frac{T_z}{(\omega_o^*)^2(I_{yy} - I_{xx}) + 2h\omega_o^* \cos 28^\circ} = 96.9 T_z \quad (17)$$

where T_z is in newton-meters. The steady-state frequency response magnitude is given by

$$|\psi_{ss}|_{T_x} = j \ 40.3 |T_x| \quad (18)$$

$$\begin{aligned} |\psi_{ss}|_{T_z} &= 286.3 |T_z| \quad \text{for } c = 2.25 \text{ (N)(m)(sec)} \\ &= 207.1 |T_z| \quad \text{for } c = 4.5 \text{ (N)(m)(sec)} \end{aligned} \quad (19)$$

where T_x and T_z are in newton-meters. As in the roll case the yaw response to T_x is 90° out of phase with the yaw response to T_z .

Results from Linearized Equations of Motion

Equations (11) to (19) may be used to estimate the satellite response to various disturbances.

Eccentricity. - Using equation (11), we find the maximum response magnitude for the worst-case eccentricity of 0.005 is

$$|\theta| = 0.0252 \text{ radian} = 1.44^\circ$$

Solar pressure. - Equations (3) to (5) are used to estimate the solar pressure effects. From equations (14) and (3), the maximum roll offset from solar pressure is

$$\varphi_{\max} = -1.027 \times 10^{-2} \text{ radian} = -0.59^\circ$$

From equations (12) and (4), the maximum constant pitch offset is

$$\theta = \pm 1.279 \times 10^{-3} \text{ radian} = \pm 0.07^\circ$$

From equations (13) and (5), the maximum pitch oscillation is

$$|\theta| = 1.94 \times 10^{-2} \text{ radian} = 1.11^\circ$$

Geometric axis misalignment. - Appendix C shows that the attitude is stable and will align the principal axes with the reference axes. The horizon sensors are aligned

with the geometric axes and will record a roll and pitch offset when the principal axes are aligned properly. From equation (1), we see that these offsets are

$$\varphi = -0.008 \text{ radian} = -0.46^\circ$$

$$\theta = 0.0024 \text{ radian} = 0.14^\circ$$

$$\psi = +0.06^\circ$$

Magnetics. - Equation (7) is used to estimate magnetic effects. Using equations (12) to (19), the satellite response to magnetic torques is

$$|\theta_{ss}| = 4.86^\circ$$

$$|\varphi_{step}| = 0.05^\circ$$

$$|\varphi_{ss}|_{T_x} = 0.74^\circ$$

$$|\varphi_{ss}|_{T_z} = -0.37^\circ j$$

$$|\psi_{step}| = 0.16^\circ$$

$$|\psi_{ss}|_{T_x} = 0.74^\circ j$$

$$|\psi_{ss}|_{T_z} = 2.64^\circ$$

Total effects. - Assuming all pitch sinusoidal disturbances are in phase, the maximum pitch frequency response amplitude is

$$|\theta_{ss}|_{\max} = 7.41^\circ$$

The maximum constant pitch offset seen by the horizon sensors consists of geometric axes misalignments and solar pressure effects

$$|\theta_{step}|_{\max} = 0.21^\circ$$

The maximum roll oscillation magnitude is

$$|\varphi_{ss}|_{\max} = 0.83^{\circ}$$

The maximum constant roll offset seen by the horizon sensors consists of geometric axes misalignments, solar pressure, and magnetic effects.

$$|\varphi_{\text{step}}|_{\max} = -1.10^{\circ}$$

The maximum yaw oscillation magnitude is

$$|\psi_{ss}|_{\max} = 2.74^{\circ}$$

The maximum constant yaw offset is

$$|\psi_{\text{step}}|_{\max} = 0.22^{\circ}$$

The response indicated above is the worst-case response found using the linearized equations of motion. The pitch frequency response magnitude appears to be the one item worthy of concern. If the magnitude is as given, only a small steady-state offset is allowed before the pitch angle exceeds the linear range of the horizon sensors ($\pm 10^{\circ}$). This is particularly important if the ion engines are initially misaligned. However, the simulated response, described in the following section, showed that the pitch oscillation magnitude is approximately 4° , a tolerable value.

Predicted Response

Appendix D briefly describes the analog and digital simulations of the satellite dynamics. If it is assumed that the satellite dipole is

$$\bar{\rho}_B = \begin{bmatrix} -9.8 \times 10^4 \\ -8.2 \times 10^4 \\ -9.8 \times 10^4 \end{bmatrix} \text{ A-cm}^2$$

and that the CMG gain is $h/c = 2.0$, the satellite steady-state attitude response was

simulated. Figure 6 shows the worst-case predicted response compared to actual flight data.

The magnitudes of the simulated attitude and CMG angles are all larger than the flight data. The simulation graph is keyed on the pitch response. So with the simulated pitch response in phase with the flight data, all other simulated responses are out of phase with the flight data.

The flight data shown in figures 6 and 7 are from one orbit during the first month of the mission. The data do not repeat exactly from one orbit to another, but the differences are minor. The magnitude of the pitch oscillation is the parameter which varies the most. The variation is less than 1° , and this may be attributed to a changing orientation of the earth's magnetic dipole. The response repeats over a 24-hour period.

The flight data are shown in steps since the parameters are sampled, and the values held for 1-minute intervals. In addition, the telemetry system quantizes the data so that pitch readings from the horizon sensors appear at 0.5° steps with the associated resolution of $\pm 0.25^\circ$. The roll steps are 0.4° and the roll resolution is $\pm 0.2^\circ$. Since the CMG gimbal angle variation is large ($\sim \pm 30^\circ$) and the allowed number of discrete steps is fixed (~ 60), the gimbal angle step size is approximately 1.20° and the resolution is 0.6° .

RESULTS FROM FLIGHT DATA

Magnetic Moment Estimation

Estimation of the satellite magnetic moment could be easily accomplished if flight data on all three Euler angles were available. Since direct measurement of the yaw angle is not possible, CMG information is used. From equations (C29), the steady-state frequency response magnitude of the CMG gimbal angle sum is given by

$$\begin{aligned} |\sigma''| &= 232.6 T_z \quad \text{for } c = 2.25 \text{ (N)(m)(sec)} \\ &= 116.6 T_z \quad \text{for } c = 4.5 \text{ (N)(m)(sec)} \end{aligned} \tag{20}$$

where $\sigma'' = \sigma_1 + \sigma_2$ and T_z is in newton-meters.

If we assume that the earth's magnetic field in the body axis system is given by equation (6), equation (A30) may be approximated by

$$\bar{T}_B = \begin{bmatrix} \rho_y(0.03915 \sin \omega_o^* t) \\ \rho_z(0.01965 \cos \omega_o^* t) - \rho_x(0.03915 \sin \omega_o^* t) \\ -\rho_y(0.01965 \cos \omega_o^* t) \end{bmatrix} \text{ dyne-cm} \quad (21)$$

where $\bar{\rho}$ is in ampere-cm² and the terms containing H_y are neglected. From equations (15) and (16) the roll frequency response magnitude is given by

$$|\varphi_{ss}| = 40.3 \sqrt{T_x^2 + T_z^2} \quad (22)$$

where T_x and T_z are in newton-meters.

Although the expected eccentricity was 0.005, the achieved eccentricity was 0.0003, hence, the pitch oscillation magnitude is assumed to be a result of magnetics and solar pressure. Ground test of CMG's showed a high probability of CMG operation near a gain of 2. Thus, assuming the CMG gain is 2.0, equations (13), (20), and (22) may be solved for the magnitude of the disturbance torques:

$$|T_y| = 5.056 \times 10^{-3} |\theta| \text{ N-m} \quad (23a)$$

$$|T_z| = 4.3 \times 10^{-3} |\sigma''| \text{ N-m} \quad (23b)$$

$$|T_x|^2 = 6.16 \times 10^{-3} |\varphi|^2 - |T_z|^2 \text{ N-m} \quad (23c)$$

Using the flight data and solving equations (23) gives

$$|T_y| = 2.38 \times 10^{-4} \text{ N-m} \quad (24a)$$

$$|T_z| = 9.53 \times 10^{-5} \text{ N-m} \quad (24b)$$

$$|T_x| = 1.97 \times 10^{-4} \text{ N-m} \quad (24c)$$

From equation (21),

$$|T_x| = 0.03915 |\rho_y|$$

and

$$|T_z| = 0.01965 |\rho_y|$$

The average of the two estimates of ρ_y is

$$|\rho_y| = 4.94 \times 10^4 \text{ A-cm}^2$$

The flight data shown in figures 6 and 7 were recorded when the sunline deviation from orbit normal was large. Thus, the pitch response is subject to both solar and magnetic torques. Since the sunline deviation was approximately 30° , the pitch torque due to solar pressure was found to be 8.85×10^{-5} newton-meter. Assuming the solar and magnetic torques are in phase, the pitch magnetic torque is

$$|T_y| = 1.495 \times 10^{-4} \text{ N-m}$$

Now assuming $|\rho_x| = |\rho_z| = \rho$,

$$|T_y| = 0.0438 \rho$$

and the initial estimates of $|\rho_x|$ and $|\rho_z|$ are

$$|\rho_x| = |\rho_z| = 3.41 \times 10^4 \text{ A-cm}^2$$

The polarity of the magnetic moments may be determined by observing the roll and pitch angles when the satellite is near the north magnetic pole and the magnetic equator. The resulting estimated total dipole is

$$\bar{\rho}_B = \begin{bmatrix} 3.41 \times 10^4 \\ -4.94 \times 10^4 \\ -3.41 \times 10^4 \end{bmatrix} \text{ A-cm}^2 \quad (25)$$

Figure 7 shows the simulated response using the estimated dipole. The figure shows good agreement of roll and pitch angles between the simulated and flight data. The simulated σ_1 response is of the proper magnitude and phase but is offset from the flight data. The offset may be due to an incorrect torquer torque level. The torquers are not regulated but are subject to temperature and current variations. The simulated σ_2 response shows the CMG input rates are sufficiently small that stiction prevents

motion. The simulated σ_2 response is offset from the flight data, but its offset is not as large as the σ_1 offset.

The dipole in equation (25) is a good approximation to the true dipole. Varying the roll and yaw magnetic moments will change the simulation from that shown in figure 7. However, these changes are of such a nature that the approximation to flight data may not be considered improved.

Using the spacecraft/SSU dipole given in appendix B, the resulting Agena/solar array dipole is

$$\bar{\rho} = \begin{bmatrix} 3.41 \times 10^4 + 2.27 \times 10^4 \\ -4.94 \times 10^4 + 1.11 \times 10^4 \\ -3.41 \times 10^4 + 2.33 \times 10^4 \end{bmatrix} = \begin{bmatrix} 5.68 \times 10^4 \\ -3.83 \times 10^4 \\ -1.08 \times 10^4 \end{bmatrix} \text{ A-cm}^2$$

Ion Engine Response

The simulations described in appendix D were used to determine acceptable ion engine thrust misalignments. It was found that if $|\alpha|$ and/or $|\beta|$ were approximately 4° with the engine operating at full thrust, the satellite's step response stability limit was exceeded and the satellite would tumble. To avoid this problem, provisions were made to allow the engines to operate at 30, 80, and 100 percent thrust levels. In addition, each engine was mounted on a gimbal system capable of correcting a thrust error as large as $\pm 10^\circ$ in the α or β axes. Thus corrections were to be made to each thrust level to avoid exceeding the stability limit.

It was found, however, that the thrust vectors were reasonably well aligned and no gimbaling of the engines was performed. If the ion thrust misalignment is small ($\alpha \leq 10^\circ$ and $\beta \leq 10^\circ$), the roll and pitch misalignment torques given in equation (A38) may be approximated by

$$T_x = -l_z F \sin \beta \quad (26a)$$

$$T_y = -F \sqrt{l_x^2 + l_z^2} \sin \alpha \cos \beta \quad (26b)$$

If the Euler angles θ and ϕ are also small, equations (12), (13), and (26) may be used to find the thrust misalignments.

Figure 8 shows the steady-state roll and pitch horizon sensor readings before and after the thrusters were started. Before the thrusters were started, the steady-state

offsets were

$$\theta = +0.20^{\circ} \quad (27a)$$

$$\varphi = -0.65^{\circ} \quad (27b)$$

The offsets were found by averaging the horizon sensor data over the orbit. After the fore thruster was started and operating at 100 percent thrust, the horizon sensor readings showed steady-state offsets of

$$\theta = -1.96^{\circ} \quad (28a)$$

$$\varphi = -1.85^{\circ} \quad (28b)$$

The offsets given in equations (27) are assumed to be the satellite response to principal axis misalignments, solar pressure, and magnetics. Thus the roll and pitch response to the thruster is

$$\theta = -2.16^{\circ} \quad (29a)$$

$$\varphi = -1.20^{\circ} \quad (29b)$$

Using equations (29), (26), and (14) and the parameters in table II gives

$$\beta = 0.51^{\circ} \quad (30)$$

Now using equations (12), (26), (29), and (30) and solving for α gives

$$\alpha = 0.48^{\circ} \quad (31)$$

After the aft thruster was started and operating at 100 percent thrust, the horizon sensor readings showed steady-state offsets of

$$\theta = +1.20^{\circ} \quad (32a)$$

$$\varphi = -0.35^{\circ} \quad (32b)$$

Following a similar procedure gives the misalignments as

$$\beta = -0.13^{\circ} \quad (33a)$$

$$\alpha = -0.22^{\circ} \quad (33b)$$

CONCLUDING REMARKS

This report has presented an analysis of the SERT II attitude response. The magnetic, solar pressure, and ion thruster torques were examined in detail. The analysis and simulation predicted an attitude response tolerable to mission objectives and did not reveal any instabilities under normal operation. The analysis, however, did show a potential instability due to thruster misalignment. The potential instability was eliminated by providing gimbaling for the ion thrusters.

Flight data compared to the predicted response showed that the analysis was correct within the tolerances on such parameters as magnetic moments, inertias, CMG gains, etc. Flight data were used to estimate the magnetic moments. The simulated response using the estimated moments showed good agreement with the flight data. Further improvement of flight and simulation data agreement is unlikely unless the earth's magnetic field model is improved and the CMG parameters are more accurately known.

Lewis Research Center,
National Aeronautics and Space Administration,
Cleveland, Ohio, April 6, 1971,
120-26.

APPENDIX A

SATELLITE ENVIRONMENT AND DISTURBANCES

To estimate or model the satellite attitude response, it is necessary to analyze the spacecraft environment and possible attitude disturbances. It was found that solar pressure torques, magnetic torques, torques from principal axes - geometric axes misalignments, and ion thruster misalignment torques would produce attitude response detectable by the onboard horizon sensors. Other sources of attitude errors were found to be negligible.

Solar Pressure

Derivation of torque equations. - For purposes of solar pressure analysis, the vehicle is considered to be a cylinder and a plate. The aft equipment rack and spacecraft geometric irregularities are ignored. References 6 and 7 give the differential force on the differential area to be

$$d\bar{F} = \left\{ (1 + R)(\hat{s} \cdot \hat{n})^2 \hat{n} + (1 - R)(\hat{s} \cdot \hat{n}) [\hat{n} \times (\hat{s} \times \hat{n})] \right\} (-P_s) dA \quad (A1)$$

The differential torque is given by

$$d\bar{T} = \bar{r}_B \times d\bar{F} \quad (A2)$$

The apparent sun motion as viewed from the spacecraft is a circle if the body angles are zero. We define an X'_B, Y'_B, Z'_B system coincident with the reference axis system at some point in the orbit such that a simple rotation about the X'_B axis places the new Y axis (Y_S) along \hat{s} . This is illustrated in figure 9. The X'_B, Y'_B, Z'_B and X_S, Y_S, Z_S systems are related by

$$\begin{bmatrix} X \\ Y \\ Z \end{bmatrix}'_B = \begin{bmatrix} 1 & 0 & 0 \\ 0 & \cos \delta & -\sin \delta \\ 0 & \sin \delta & \cos \delta \end{bmatrix} \begin{bmatrix} X \\ Y \\ Z \end{bmatrix}_S \quad (A3)$$

The reference system and the X'_B, Y'_B, Z'_B system are related by

$$\begin{bmatrix} X \\ Y \\ Z \end{bmatrix}_R = \begin{bmatrix} \cos(\omega_0 t + \gamma) & 0 & \sin(\omega_0 t + \gamma) \\ 0 & 1 & 0 \\ -\sin(\omega_0 t + \gamma) & 0 & \cos(\omega_0 t + \gamma) \end{bmatrix} \begin{bmatrix} X \\ Y \\ Z \end{bmatrix}_B \quad (A4)$$

where γ is used as a phase angle to relate the systems in time.

The unit vector \hat{s} in the S system is given by

$$\hat{s} = \begin{bmatrix} 0 \\ 1 \\ 0 \end{bmatrix}$$

Thus, in the reference system, the vector \hat{s} becomes

$$\hat{s}_R = \begin{bmatrix} \sin \delta \sin(\omega_0 t + \gamma) \\ \cos \delta \\ \sin \delta \cos(\omega_0 t + \gamma) \end{bmatrix}$$

By using equation (2) and assuming that the body rotation angles are small, a vector in the reference system may be found in the body system by

$$\begin{bmatrix} x \\ y \\ z \end{bmatrix} = \begin{bmatrix} 1 & \psi & -\theta \\ -\psi & 1 & \varphi \\ \theta & -\varphi & 1 \end{bmatrix} \begin{bmatrix} X \\ Y \\ Z \end{bmatrix}_R$$

Thus, in the body system, the vector \hat{s} becomes

$$\hat{s}_B = \begin{bmatrix} S\delta \sin(\omega_0 t + \gamma) + \psi C\delta - \theta S\delta \cos(\omega_0 t + \gamma) \\ -\psi S\delta \sin(\omega_0 t + \gamma) + C\delta + \varphi S\delta \cos(\omega_0 t + \gamma) \\ \theta S\delta \sin(\omega_0 t + \gamma) - \varphi C\delta + S\delta \cos(\omega_0 t + \gamma) \end{bmatrix} \quad (A5)$$

For the solar panels, the vector \hat{n} in the body system is

$$\hat{n}_B = \begin{bmatrix} -0.0010 \\ 1.0000 \\ -0.0080 \end{bmatrix}$$

Thus, $\hat{s}_B \times \hat{n}_B = -0.001 S_x + S_y - 0.008 S_z$ and

$$\hat{n}_B \times (\hat{s}_B \times \hat{n}_B) = \begin{bmatrix} S_x(1 + 6.4 \times 10^{-5}) + 1 \times 10^{-3} S_y - 8 \times 10^{-6} S_z \\ 1 \times 10^{-3} S_x + 6.5 \times 10^{-5} S_y + 8 \times 10^{-3} S_z \\ -8 \times 10^{-6} S_x + 8 \times 10^{-3} S_y + S_z(1 + 10^{-6}) \end{bmatrix}$$

where S_x , S_y , S_z are given by equation (A5). Substituting in equation (A1) and integrating over the area gives

$$\bar{F}_B = -P_s A (S_y - 0.001 S_x - 0.008 S_z) \left\{ \begin{array}{l} (1 + R)(S_y - 0.001 S_x - 0.008 S_z)(-0.001) \\ \quad + (1 - R)[S_x(1 + 6.4 \times 10^{-5}) + 1 \times 10^{-3} S_y - 8 \times 10^{-6} S_z] \\ (1 + R)(S_y - 0.001 S_x - 0.008 S_z) \\ \quad + (1 - R)(6.5 \times 10^{-5} S_y + 1 \times 10^{-3} S_x + 8 \times 10^{-3} S_z) \\ (1 + R)(S_y - 0.001 S_x - 0.008 S_z)(-0.008) \\ \quad + (1 - R)[S_z(1 + 10^{-6}) + 8 \times 10^{-3} S_y - 8 \times 10^{-6} S_x] \end{array} \right\} \quad (A6)$$

The solar panels are offset in the +Y geometric axis direction. Thus, the radius vector to the panels' center of pressure in the geometric system is

$$r_G = \begin{bmatrix} 0 \\ r_{GY} \\ r_{GZ} \end{bmatrix}$$

Using equation (1) the radius vector in the body system is

$$\bar{\mathbf{r}}_B = \begin{bmatrix} -0.001 r_{GY} + 0.0024 r_{GZ} \\ r_{GY} + 0.008 r_{GZ} \\ -0.008 r_{GY} + r_{GZ} \end{bmatrix} = \begin{bmatrix} r_x \\ r_y \\ r_z \end{bmatrix}$$

and the torque on the body due to solar pressure on the solar panels is

$$\bar{\mathbf{T}}_B = \hat{\mathbf{x}}(r_y F_z - r_z F_y) + \hat{\mathbf{y}}(r_z F_x - r_x F_z) + \hat{\mathbf{z}}(r_x F_y - r_y F_x) \quad (\text{A7})$$

To determine the solar pressure forces on the Agena and the spacecraft, we introduce an additional coordinate system. The $\hat{\mathbf{i}}, \hat{\mathbf{j}}, \hat{\mathbf{k}}$ system shown in figure 10 is a right-handed coordinate system with the origin at the center of mass and with $\hat{\mathbf{k}}$ along the axis of the cylinder, $\hat{\mathbf{i}}$ directed away from $\hat{\mathbf{s}}$ such that the $\hat{\mathbf{i}}\text{-}\hat{\mathbf{k}}$ plane contains $\hat{\mathbf{s}}$, and $\hat{\mathbf{j}}$ completes the set such that $\hat{\mathbf{j}} \cdot \hat{\mathbf{s}} = 0$. The angles α' and β' are defined in figure 10.

In the $\hat{\mathbf{i}}, \hat{\mathbf{j}}, \hat{\mathbf{k}}$ system

$$\hat{\mathbf{n}} = \begin{bmatrix} -\sin \alpha' \\ -\cos \alpha' \\ 0 \end{bmatrix}$$

and

$$\hat{\mathbf{s}} = \begin{bmatrix} -\cos \beta' \\ 0 \\ -\sin \beta' \end{bmatrix}$$

The differential area is given by $dA = r' d\alpha' dh'$. Thus, equation (A1) becomes

$$d\bar{F} = -P_s \left\{ (1 + R)(\cos \beta' \sin \alpha')^2 \begin{bmatrix} -\sin \alpha' \\ -\cos \alpha' \\ 0 \end{bmatrix} + (1 - R)(\cos \beta' \sin \alpha') \begin{bmatrix} -\cos^2 \alpha' \cos \beta' \\ \sin \alpha' \cos \alpha' \cos \beta' \\ -\sin \beta' \end{bmatrix} \right\} r' d\alpha' dh' \quad (A8)$$

The moment arm to the differential area in the $\hat{i}, \hat{j}, \hat{k}$ system is

$$r_B = \begin{bmatrix} -r' \sin \alpha' \\ -r' \cos \alpha' \\ r_k \end{bmatrix}$$

Thus, the differential torque from the differential area is

$$d\bar{T} = \hat{i}(-r' \cos \alpha' dF_k - r_k dF_j) + \hat{j}(r_k dF_i + r' \sin \alpha' dF_k) + \hat{k}(-r' \sin \alpha' dF_j + r' \cos \alpha' dF_i) \quad (A9)$$

where the components of dF are given in equation (A8).

Integrating over the area exposed to sunlight gives the torque in the $\hat{i}, \hat{j}, \hat{k}$ system:

$$\bar{T} = \hat{i}(0) + \hat{j} \left\{ P_s r' \cos \beta' h' \left[r_k \cos \beta' \left(2 + \frac{2}{3} R \right) + \frac{\pi}{2} r' (1 - R) \sin \beta' \right] \right\} + \hat{k}(0) \quad (A10)$$

Now, a vector in the $\hat{i}, \hat{j}, \hat{k}$ system may be found in the geometric system

$$\begin{bmatrix} X \\ Y \\ Z \end{bmatrix}_G = \begin{bmatrix} -\sin\left(\tan^{-1} \frac{S_{GX}}{S_{GY}}\right) & -\cos\left(\tan^{-1} \frac{S_{GX}}{S_{GY}}\right) & 0 \\ -\cos\left(\tan^{-1} \frac{S_{GX}}{S_{GY}}\right) & \sin\left(\tan^{-1} \frac{S_{GX}}{S_{GY}}\right) & 0 \\ 0 & 0 & -1 \end{bmatrix} \begin{bmatrix} i \\ j \\ k \end{bmatrix} \quad (A11)$$

where S_{GX} and S_{GY} are the X and Y components of \hat{s} in the geometric system. Using equation (1) we find

$$S_{GX} = S_x + 0.001 S_y - 0.0024 S_z$$

$$S_{GY} = S_y - 0.001 S_x - 0.008 S_z$$

where S_x , S_y , S_z are the components of \hat{s} in the body system and given in equation (A5).

Using equations (A10) and (A11) we find the torque in the geometric system:

$$\begin{aligned} T_G = & \hat{X}_G \left(-\cos\left(\tan^{-1} \frac{S_{GX}}{S_{GY}}\right) \left\{ P_s r' \cos \beta' h' \left[r_k \cos \beta' \left(2 + \frac{2}{3} R \right) + \frac{\pi}{2} r' (1 - R) \sin \beta' \right] \right\} \right) \\ & + \hat{Y}_G \left(\sin\left(\tan^{-1} \frac{S_{GX}}{S_{GY}}\right) \left\{ P_s r' \cos \beta' h' \left[r_k \cos \beta' \left(2 + \frac{2}{3} R \right) + \frac{\pi}{2} r' (1 - R) \sin \beta' \right] \right\} \right) + \hat{Z}_G(0) \end{aligned} \quad (A12)$$

where

$$\sin \beta' = \hat{Z}_G \cdot \hat{s}_G = S_z + 0.0024 S_x + 0.008 S_y$$

and

$$\cos \beta' = \sqrt{1 - \sin^2 \beta'}$$

Using equations (1) and (A12) we find the torque in the body system to be

$$\overline{T}_B = \hat{x}(T_{GX} - 0.001 T_{GY}) + \hat{y}(T_{GY} + 0.001 T_{GX}) + \hat{z}(-0.0024 T_{GX} - 0.008 T_{GY}) \quad (A13)$$

Equations (A7) and (A13) give the total solar pressure torque on the satellite.

Approximate torque equations. - Estimation of the solar pressure torque is not easily accomplished with the equations given. To estimate the torque from solar pressure on the solar array we first assume that \hat{n}_B is given by

$$\hat{n}_B = \begin{bmatrix} 0 \\ 1 \\ 0 \end{bmatrix}$$

then

$$\hat{s}_B \cdot \hat{n}_B = S_y$$

and

$$\hat{n}_B \times (\hat{s}_B \times \hat{n}_B) = \begin{bmatrix} S_x \\ 0 \\ S_z \end{bmatrix}$$

The components S_x and S_z are given in equation (A5). Using these approximations, equation (A6) become

$$\overline{F}_B = -P_s A S_y \begin{bmatrix} (1 - R)S_x \\ (1 + R)S_y \\ (1 - R)S_z \end{bmatrix} \quad (A14)$$

Since we limit the sun declination to 30° or less, $|F_y|$ will always be larger than $|F_x|$ or $|F_z|$. We may not, however, eliminate F_x or F_z from the approximation. Since the panels' reflectivity is small ($R \sim 0.2$), when $\delta \sim 30^\circ$ the force components are all the same order of magnitude.

For SERT II, the moment arm to the panels' center of pressure in the geometric system is

$$\bar{r}_G = \begin{bmatrix} 0 \\ r_{GY} \\ r_{GZ} \end{bmatrix} = \begin{bmatrix} 0 \\ 0.20 \\ -3.35 \end{bmatrix} \text{ meters or } \begin{bmatrix} 0 \\ 0.67 \\ -11.0 \end{bmatrix} \text{ ft}$$

In the body system, the moment arm becomes

$$\begin{aligned} \bar{r}_B &= \begin{bmatrix} -0.008 \\ 0.18 \\ -3.35 \end{bmatrix} \text{ or } \sim \begin{bmatrix} 0 \\ 0 \\ -3.35 \end{bmatrix} \text{ meters} \\ &= \begin{bmatrix} -0.027 \\ 0.58 \\ -11.0 \end{bmatrix} \text{ or } \sim \begin{bmatrix} 0 \\ 0 \\ -11 \end{bmatrix} \text{ ft} \end{aligned}$$

Using the approximation to r_B , equation (A7) becomes

$$\bar{T}_B = \hat{x}(-r_Z F_Y) + \hat{y}(r_Z F_X) + \hat{z}(0) \quad (A15)$$

Noting that the Euler angles are small, we may approximate the force components as

$$F_X \sim -P_S A(1 - R) \left[C\delta S\delta S(\omega_o t + \gamma) + \psi C^2\delta \right] \quad (A16a)$$

$$F_Y \sim -P_S A(1 + R)C^2\delta \quad (A16b)$$

where we have retained the most significant terms.

Letting

$$A = 17.65 \text{ m}^2 (190 \text{ ft}^2)$$

$$P_s = 4.788 \times 10^{-6} \text{ N/m}^2 (1 \times 10^{-7} \text{ lb/ft}^2)$$

$$\psi = \pm 0.1$$

$$R = 0.2$$

we find that the maximum constant roll torque occurs when $\delta = 0$ and is

$$T_x = -3.40 \times 10^{-4} \text{ N-m} = -2.51 \times 10^{-4} \text{ ft-lb}$$

The maximum constant pitch torque also occurs when $\delta = 0$ and $\psi = \pm 0.1$ and is

$$T_y = \pm 2.26 \times 10^{-5} \text{ N-m} = \pm 1.67 \times 10^{-5} \text{ ft-lb}$$

The sinusoidal pitch torque of maximum magnitude occurs when $\delta = 30^\circ$ and is

$$\begin{aligned} T_y &= 9.82 \times 10^{-5} \sin(\omega_o^* t + \gamma) \text{ N-m} \\ &= 7.24 \times 10^{-5} \sin(\omega_o^* t + \gamma) \text{ ft-lb} \end{aligned}$$

The roll torque for $\delta = 30^\circ$ becomes

$$\begin{aligned} T_x &= -2.55 \times 10^{-4} \text{ N-m} \\ &= -1.88 \times 10^{-4} \text{ ft-lb} \end{aligned}$$

These expressions provide an estimate of the torque due to solar pressure on the solar panels.

To estimate the solar pressure effects on the Agena and spacecraft, we first assume that the Euler angles may be neglected. Then the following relations apply:

$$\frac{S_{GX}}{S_{GY}} \sim \frac{S_x}{S_y} = \tan \delta \sin(\omega_o^* t + \gamma)$$

$$-\cos \left(\tan^{-1} \frac{S_{GX}}{S_{GY}} \right) = \frac{-\cos \delta}{\sqrt{1 - C^2(\omega_o^* t + \gamma) S^2 \delta}}$$

$$\sin \left(\tan^{-1} \frac{S_{GX}}{S_{GY}} \right) = \frac{S \delta \sin(\omega_o^* t + \gamma)}{\sqrt{1 - S^2 \delta C^2(\omega_o^* t + \gamma)}}$$

$$\sin \beta' = S \delta C(\omega_o^* t + \gamma)$$

$$\cos \beta' = \sqrt{1 - S^2 \delta C^2(\omega_o^* t + \gamma)}$$

We also assume that equation (A13) may be approximated by

$$\bar{T}_B = \begin{bmatrix} T_{GX} \\ T_{GY} \\ 0 \end{bmatrix} = \begin{bmatrix} T_x \\ T_y \\ 0 \end{bmatrix}$$

Now letting

$$r' = 0.76 \text{ m (2.5 ft)}$$

$$r_k = -0.36 \text{ m (-1.17 ft)}$$

$$P_s = 4.788 \times 10^{-6} \text{ N/m}^2 (1 \times 10^{-6} \text{ lb/ft}^2)$$

$$R = 0.8$$

$$2r'h' = 9.01 \text{ m}^2 (97 \text{ ft}^2)$$

and using these relations, we find T_x and T_y from equation (A12). For $\delta = 0$, the torque due to solar pressure on the Agena-spacecraft is

$$T_x \sim 1.95 \times 10^{-5} \text{ N-m} = 1.44 \times 10^{-5} \text{ ft-lb}$$

$$T_y \sim 0$$

For $\delta = 30^\circ$, the roll and pitch torques from solar pressure on the Agena-spacecraft can be approximated by

$$T_x = 1.69 \times 10^{-5} \text{ N-m} - 2.24 \times 10^{-6} \cos(\omega_o^* t + \gamma) \text{ N-m}$$

$$= 1.25 \times 10^{-5} \text{ ft-lb} - 1.65 \times 10^{-6} \cos(\omega_o^* t + \gamma) \text{ ft-lb}$$

$$T_y = -9.76 \times 10^{-6} \sin(\omega_o^* t + \gamma) \text{ N-m}$$

$$= -7.2 \times 10^{-6} \sin(\omega_o^* t + \gamma) \text{ ft-lb}$$

It is evident from the previous calculations that the torques from solar pressure on the Agena-spacecraft are an order of magnitude less than the torques from solar pressure on the solar array. In addition, for $\delta = 0$, the Agena-spacecraft roll torque is opposite in sign from the solar array roll torque. For $\delta = 30^\circ$, the constant components of the roll torques are of opposite sign, while the pitch torques are 180° out of phase. The approximations indicate that solar pressure torques on the Agena-spacecraft tend to lessen the torques from the solar array. Thus, for crude analysis purposes, neglecting the Agena-spacecraft solar pressure torques would provide a worst case.

Magnetics

The instantaneous magnetic torque on the satellite is given by

$$\bar{T} = \bar{\rho} \times \bar{H} \quad (\text{A17})$$

where $\bar{\rho}$ is the satellite dipole and \bar{H} is the earth field vector. If ρ is given in amperes-cm² and H is oersteds, the torque is given in dyne-cm by

$$\bar{T} = \frac{1}{10} (\bar{\rho} \times \bar{H}) \quad (\text{A18})$$

To find the torque in the body (principal) axis system, several coordinate definitions and transformations are needed. We define an earth-centered inertial coordinate system X_I, Y_I, Z_I with X_I pointing toward the vernal equinox, Z_I along the earth-spin axis, and Y_I completing the right-handed set. We also define an earth-centered "magnetic" coordinate system X_M, Y_M, Z_M with X_M pointing toward the 0° longitude point on the equator, Z_M positive northward and rotated 18° from the earth-spin axis about X_M , and Y_M completing the right-handed set. The two coordinate systems are related by the transformation:

$$\begin{bmatrix} X \\ Y \\ Z \end{bmatrix}_I = \begin{bmatrix} C\Omega_E & -S\Omega_E C18^\circ & S\Omega_E S18^\circ \\ S\Omega_E & C\Omega_E C18^\circ & -C\Omega_E S18^\circ \\ 0 & S18^\circ & C18^\circ \end{bmatrix} \begin{bmatrix} X \\ Y \\ Z \end{bmatrix}_M \quad (A19)$$

where Ω_E is the inertial longitude of the Greenwich meridian.

Since the earth's field is an assumed dipole with axis Z_M , we can express the field at the location of the satellite in terms of two components. The axial component is that component parallel to the dipole axis. The normal component is perpendicular to the axial component and directed from the satellite toward the earth's dipole axis. Figure 11 shows the unit axial and normal vectors. When the unit vectors are defined in this manner, reference 8 gives the magnitude of the axial and normal components in oersteds as

$$H_{ax} = 0.308 \frac{1 - 3 \cos^2 \eta}{\left(\frac{r_c}{R_E}\right)^3}$$

$$H_{norm} = 0.461 \frac{\sin 2\eta}{\left(\frac{r_c}{R_E}\right)^3}$$

where η is the angle between the dipole axis and the radius vector to the satellite. The magnitude of \bar{H} is

$$|\bar{H}| = \sqrt{H_{ax}^2 + H_{norm}^2}$$

We now define an earth-centered orbit system X_O, Y_O, Z_O such that X_O is along the line of nodes and positive toward the ascending node, Z_O is positive along the orbit angular momentum vector, and Y_O completes the right-handed set. The orbit and inertial systems are related by

$$\begin{bmatrix} X \\ Y \\ Z \end{bmatrix}_O = \begin{bmatrix} C\Omega & S\Omega & 0 \\ -S\Omega \cos i & C\Omega \cos i & \sin i \\ S\Omega \sin i & -C\Omega \sin i & \cos i \end{bmatrix} \begin{bmatrix} X \\ Y \\ Z \end{bmatrix}_I \quad (A21)$$

Where Ω is the inertial longitude of the orbit ascending node and i is the inclination ($i = 99.1$ for SERT II). The absence of a phase angle does not restrict the analysis. The inertial, magnetic, and orbit coordinate systems are shown in figure 12. The reference axis system (defined previously) and the orbit system are related by

$$\begin{bmatrix} X \\ Y \\ Z \end{bmatrix}_R = \begin{bmatrix} -\sin \omega_o t & \cos \omega_o t & 0 \\ 0 & 0 & -1 \\ -\cos \omega_o t & -\sin \omega_o t & 0 \end{bmatrix} \begin{bmatrix} X \\ Y \\ Z \end{bmatrix}_O \quad (A22)$$

The unit vector along the magnetic dipole axis is given in the magnetic coordinate system as

$$\hat{H}_{ax} = \begin{bmatrix} 0 \\ 0 \\ 1 \end{bmatrix}$$

Using equation (A19) \hat{H}_{ax} in the inertial system is found to be

$$\hat{H}_{ax} = \begin{bmatrix} S\Omega_z \sin 18^\circ \\ -C\Omega_z \sin 18^\circ \\ \cos 18^\circ \end{bmatrix}$$

Using equation (A21), \hat{H}_{ax} in the orbit system is

$$\hat{H}_{ax} = \begin{bmatrix} S18^0 S(\Omega_E - \Omega) \\ -S18^0 Ci C(\Omega_E - \Omega) + Si C18^0 \\ S18^0 Si C(\Omega_E - \Omega) + Ci C18^0 \end{bmatrix}$$

Using equation (A23), \hat{H}_{ax} in the reference system is

$$\hat{H}_{ax} = \begin{bmatrix} -S\omega_o t S18^0 S(\Omega_E - \Omega) + C\omega_o t(-S18^0 Ci C(\Omega_E - \Omega) + Si C18^0) \\ -S18^0 Si C(\Omega_E - \Omega) - Ci C18^0 \\ -C\omega_o t S18^0 S(\Omega_E - \Omega) - S\omega_o t(-S18^0 Ci C(\Omega_E - \Omega) + Si C18^0) \end{bmatrix}$$

or

$$\hat{H}_{ax} = \begin{bmatrix} H_1 \\ H_2 \\ H_3 \end{bmatrix}$$

Now in the reference axis system, the unit radius vector from earth center to the spacecraft is given by

$$\hat{r}_R = \begin{bmatrix} 0 \\ 0 \\ -1 \end{bmatrix}$$

Thus, $\cos \eta$ can be found by

$$\cos \eta = H_{ax} \cdot r_R = -H_3 = C\omega_o t S18^0 S(\Omega_E - \Omega) + S\omega_o t(-S18^0 Ci C(\Omega_E - \Omega) + Si C18^0) \quad (A24)$$

The unit normal vector H_{norm} , as shown in figure 11, is perpendicular to \hat{H}_{ax} and directed from the satellite to the dipole axis. Thus, $\hat{H}_{norm} \sin \eta$ is given by

$$\hat{H}_{\text{norm}} \sin \eta = \hat{H}_{\text{ax}} \times (\hat{H}_{\text{ax}} \times \hat{r}_R) \quad (\text{A25})$$

and

$$\hat{H}_{\text{norm}} \sin \eta = \begin{bmatrix} -H_1 H_3 \\ -H_2 H_3 \\ H_1^2 + H_2^2 \end{bmatrix} \quad (\text{A26})$$

where H_1, H_2, H_3 are given in equation (A23).

Now, using equations (A20), (A23), (A24), and (A26), we find the earth's magnetic field in the reference system:

$$\bar{H}_R = \left(\frac{R_E}{r_c} \right)^3 \begin{bmatrix} 0.308 (1 - 3H_3^2) H_1 + 0.922(-H_3)(-H_1 H_3) \\ 0.308 (1 - 3H_3^2) H_2 + 0.922(-H_3)(-H_2 H_3) \\ 0.308 (1 - 3H_3^2) H_3 + 0.922(-H_3)(H_1^2 + H_2^2) \end{bmatrix} \quad (\text{A27})$$

or

$$\bar{H}_R = \left(\frac{R_E}{r_c} \right)^3 \begin{bmatrix} H_1 (0.308 - 0.002 H_3^2) \\ H_2 (0.308 - 0.002 H_3^2) \\ H_3 (0.614 - 0.002 H_3) \end{bmatrix}$$

and since $H_{3, \text{max}} = 1$ we may approximate \bar{H}_R by

$$\bar{H}_R = \left(\frac{R_E}{r_c} \right)^3 \begin{bmatrix} 0.308 H_1 \\ 0.308 H_2 \\ -0.614 H_3 \end{bmatrix} \quad (\text{A28})$$

For the SERT II expected orbit parameters given in table I, equation (A28) becomes

$$\bar{H}_R = \begin{bmatrix} -0.0614 S\omega_o t S(\Omega_E - \Omega) + C\omega_o t (0.00972 C(\Omega_E - \Omega) + 0.1867) \\ -0.0607 C(\Omega_E - \Omega) + 0.0299 \\ 0.122 C\omega_o t S(\Omega_E - \Omega) + S\omega_o t (0.0194 C(\Omega_E - \Omega) + 0.372) \end{bmatrix} \quad (A29)$$

Now, if the Euler angles are small, $\bar{H}_B \sim \bar{H}_R$. If the satellite dipole is expressed as

$$\rho = \begin{bmatrix} \rho_x \\ \rho_y \\ \rho_z \end{bmatrix}$$

from equation (A18) the magnetic torque on the body is

$$T_B = \frac{1}{10} \begin{bmatrix} \rho_y H_z - \rho_z H_y \\ \rho_z H_x - \rho_x H_z \\ \rho_x H_y - \rho_y H_x \end{bmatrix} \quad (A30)$$

where H_x , H_y , H_z are given by equation (A29).

For analysis purposes, equation (A29) may be approximated by

$$\bar{H}_R = \begin{bmatrix} 0.1965 \cos \omega_o^* t \\ 0.03 \\ 0.3915 \sin \omega_o^* t \end{bmatrix} \text{ oersteds} \quad (A31)$$

where we have approximated the instantaneous orbit rate ω_o by the average orbit rate ω_o^* , let $\Omega_E - \Omega = 90^\circ$, and ignored the phase angles.

Ion Thruster Misalignment

Figure 13 shows a schematic of the geometric and thruster axis systems. The $x_{T,A}$, $y_{T,A}$, $z_{T,A}$ system is the reference system for the aft ion thruster. Similarly, the $x_{T,F}$, $y_{T,F}$, $z_{T,F}$ system is the reference system for the fore thruster. In both

thruster reference systems, the x_T axis is directed through the center of mass. The desired thrust direction is along x_T .

The thrust misalignment is found in terms of the α and β angular errors defined by figure 13. The x'', y'', z'' system is related to the x_T, y_T, z_T system by:

$$\begin{bmatrix} x \\ y \\ z \end{bmatrix}_T = \begin{bmatrix} C\alpha C\beta & -C\alpha S\beta & S\alpha \\ S\beta & C\beta & 0 \\ -S\alpha C\beta & S\alpha S\beta & C\alpha \end{bmatrix} \begin{bmatrix} x'' \\ y'' \\ z'' \end{bmatrix} \quad (A32)$$

It is assumed that the true ion engine thrust is along the x'' axis, and thus,

$$\bar{F}'' = \begin{bmatrix} F \\ 0 \\ 0 \end{bmatrix} \quad (A33)$$

Using equation (A32) we find \bar{F} in the thruster reference system:

$$\bar{F}_T = \begin{bmatrix} F C\alpha C\beta \\ F S\beta \\ -F S\alpha C\beta \end{bmatrix} \quad (A34)$$

Now the thruster reference system is related to the geometric system by

$$\begin{bmatrix} x \\ y \\ z \end{bmatrix}_G = \begin{bmatrix} \frac{-l_x}{\sqrt{l_x^2 + l_z^2}} & 0 & \frac{l_z}{\sqrt{l_x^2 + l_z^2}} \\ 0 & 1 & 0 \\ \frac{-l_z}{\sqrt{l_x^2 + l_z^2}} & 0 & \frac{-l_x}{\sqrt{l_x^2 + l_z^2}} \end{bmatrix} \begin{bmatrix} X \\ Y \\ Z \end{bmatrix}_T \quad (A35)$$

where l_x and l_z are defined in figure 13 and their values given in table II. Using equation (A35), the thrust in the geometric system is

$$\bar{\mathbf{F}}_G = \begin{bmatrix} \frac{-l_x F C\alpha C\beta - l_z F S\alpha C\beta}{\sqrt{l_x^2 + l_z^2}} \\ F S\beta \\ \frac{-l_z F C\alpha C\beta + l_x F S\alpha C\beta}{\sqrt{l_x^2 + l_z^2}} \end{bmatrix} \quad (\text{A36})$$

The radius vector to the point of thrust application is given in the geometric system as

$$\bar{\mathbf{r}}_G = \begin{bmatrix} l_x \\ 0 \\ l_z \end{bmatrix}$$

Thus the torque due to thrust misalignment in the geometric system is

$$\bar{\mathbf{T}}_G = \begin{bmatrix} -l_z F \sin \beta \\ -F \sqrt{l_x^2 + l_z^2} \sin \alpha \cos \beta \\ l_x F \sin \beta \end{bmatrix} \quad (\text{A37})$$

Thus, using equation (1) we find the principal axis torques due to thrust misalignment are

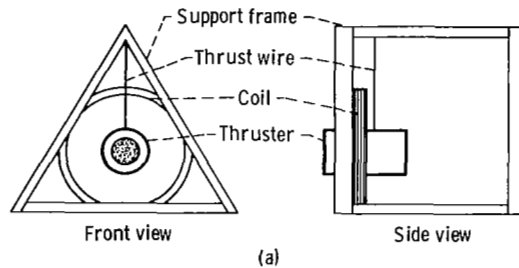
$$\bar{\mathbf{T}}_B = \begin{bmatrix} -l_z F \sin \beta + 0.001 F \sqrt{l_x^2 + l_z^2} \sin \alpha \cos \beta + 0.0024 F l_x \sin \beta \\ -0.001 F l_z \sin \beta - F \sqrt{l_x^2 + l_z^2} \sin \alpha \cos \beta + 0.008 l_x F \sin \beta \\ 0.0024 l_z F \sin \beta - 0.008 F \sqrt{l_x^2 + l_z^2} \sin \alpha \cos \beta + l_x F \sin \beta \end{bmatrix} \quad (\text{A38})$$

APPENDIX B

MAGNETIC DIPOLE MOMENT MEASUREMENTS ON THE SERT II SPACECRAFT AND SSU

To permit the determination of the magnetically caused disturbance torques acting on SERT II, it was necessary to obtain an estimate of the net magnetic dipole moment of the satellite in its orbital configuration. This configuration can be separated into two parts for purposes of discussing the magnetic measurements which were made. The first part comprised the Agena stage and the solar array, for which estimates of the residual dipole moments were obtained from the Agena contractor. The second part consists of the spacecraft (S/C) and spacecraft support unit (SSU), which were either fabricated or integrated at Lewis and were, therefore, available for magnetic testing. The remainder of this discussion is concerned with measurements made on this latter part of the orbital configuration.

Because the ion thrusters each contain several permanent magnets, it was expected that they would represent the largest single contributor to the net magnetic dipole moment. An experimental setup was, therefore, devised to measure this dipole (see sketch a). The setup consisted of a large-diameter coil of copper wire of essentially



zero length. The thruster was suspended by a torsion wire so that the center of the effective magnetic dipole was as close to the center of the coil as possible. The entire setup was aligned with the coil plane vertical and perpendicular to magnetic north. When a current of the proper polarity was passed through the coil, the period of oscillation of the suspended thruster was given by

$$\tau = 2\pi \sqrt{\frac{I}{K_W + 10^{-8} \rho_T (H_C + H_E)}} \quad (B1)$$

where

- H_E horizontal magnetic field intensity component of the earth, oersteds
 H_C magnetic field intensity due to current at center of coil, oersteds
 I moment of inertia of suspended assembly, kg-m²
 K_W torsional spring constant of suspension wire, N-m/rad
 ρ_T magnitude of magnetic dipole moment of thruster, A-cm²

With no current in the coil, the period is given by

$$\tau' = 2\pi \sqrt{\frac{I}{K_W + 10^{-8} \rho_T H_E}} \quad (B2)$$

Combining equations (B1) and (B2) gives

$$\rho_T = \frac{10^8 K_W \left[\left(\frac{\tau'}{\tau} \right)^2 - 1 \right]}{H_C - H_E \left[\left(\frac{\tau'}{\tau} \right)^2 - 1 \right]}$$

The value of K_W was obtained by suspending a known moment of inertia from the wire and observing the period. This method was used to obtain the value of the dipole moment of a flight prototype thruster by suspending it in turn about each of the three principal axes. The dipole was found to be very nearly parallel to the thrust axis of the thruster and to have a magnitude of about 23×10^4 ampere-cm². (One A-cm² normal to a magnetic field intensity of 1 Oe has 10^{-8} N-m of torque exerted on it.)

Measurements on Overall Spacecraft-SSU

Because of its large size and weight, methods which required dynamic motion of the S/C-SSU combination, such as the torsion wire method previously described, were felt to be impractical. Instead, it was decided that field measurement techniques would be used to obtain a value for the overall magnetic dipole moment of the combination.

The magnetic field intensity along the axis of a magnetic dipole is given by the following expression:

$$H = \frac{2\rho r}{(r^2 - l^2)^2}$$

where ρ is the magnitude of the magnetic dipole moment, r is the axial distance from the center of the dipole to the point of measurement, and l is the length of the dipole. If l is assumed to be small compared to the measurement distance, a very simple expression results for the magnetic intensity:

$$H = \frac{2\rho}{r^3}$$

Thus, if the spacecraft is assumed to contain a single dipole of negligible length, an estimate of the magnitude of that dipole can be obtained by measuring the magnetic intensity at a specified distance. This method was used to determine the dipole magnitude for the SERT II S/C-SSU combination.

In the actual case, the S/C-SSU contains not one but several magnetic dipoles, each located in a different place within the combination. If the measurement distance is made sufficiently large, however, the dipole magnitude determined will be that of a single equivalent dipole. Since the torques produced by the interaction of the earth's magnetic field with each of the actual dipoles are vectorially additive, determination of the magnitude of the single equivalent dipole is sufficient to establish the values of magnetic torque acting upon the satellite.

The S/C-SSU combination was mounted in a fixture which allowed it to be both rotated about all three principal axes and translated horizontally. A sensitive magnetometer was mounted on a tripod with the probe sensitive axis horizontal. The measurement procedure was as follows: With an S/C-SSU principal axis in line with the magnetometer probe and as far from it as possible, the magnetometer was set to its most sensitive scale and any ambient field readings were biased out. The S/C-SSU combination was then moved toward the probe until a specified field reading was obtained. The distance from the center of the combination to the center of the probe was measured. The combination was then moved away as far as possible, rotated through 180° to orient the negative of the same principal axis toward the probe, and the preceding steps repeated. This procedure was repeated for the other two principal axes. Both positive and negative readings were taken on each principal axis to account for any offset of the center of the equivalent dipole from the center of the S/C-SSU combination. The positive and negative distance readings were averaged.

Results

The torsional pendulum setup was used to determine the magnetic dipole moment of a flight prototype thruster, since these were expected to be the largest single contributor to the net dipole moment. The values obtained for this thruster are shown in table III. Also measured were several of the individual bar magnets which are used in the thrusters themselves. The values obtained for these magnets averaged to about 3.4×10^4 ampere-cm². As can be seen from the table, the main thruster dipole moment is essentially parallel to the thrust axis and has a magnitude of approximately 2.3×10^5 ampere-cm². With the two thrusters mounted on the spacecraft in their nominal orientations, the thruster magnets have their N-poles aligned toward the thruster exit on the orbit-raising thruster, while the N-poles are aligned away from the thruster exit for the orbiting-lowering thruster. With this configuration, the net yaw-axis component is zero, while the net roll-axis component is about 7.6×10^4 ampere-cm². To reduce the residual roll dipole to near zero, two thruster magnets having a total dipole of 6.8×10^4 ampere-cm², were attached to the S/C parallel to the roll axis.

As a check on these results, the field measurement method was used to again determine the dipole magnitude of the flight prototype thruster, as well as the actual flight thrusters and the overall S/C-SSU combination. The results of these determinations are also presented in table III. It will be seen that the prototype value obtained by this method is about 22 percent higher than that obtained using the torsional pendulum setup. It is felt that the field measurement technique produces the more accurate value, and that the difference can be mainly attributed to the nonlinearity of the magnetic field lines for points outside the coil plane. In any case, the values are sufficiently close that assurance was gained as to the adequacy of the dipole compensation previously described.

Measurements were made on the spacecraft-SSU combination in both the unpowered and powered configurations, to determine the contribution of any uncompensated current loops to the overall dipole. As can be seen from table III, these values are quite small compared to those which arise from permanent magnetism. It can also be seen that compensation by the two thruster magnets in the roll axis is adequate, although not as good as originally expected. This also indicates that the field measurement technique produced a more accurate value for the thruster dipole.

The values received from the Agena contractor for the Agena vehicle and solar array dipoles were 6.0×10^4 and 1.5×10^4 ampere-cm², respectively. No polarities were provided with these numbers and so they were assumed to add in worst-case fashion. Finally, an estimate based on solar array circuit diagrams indicated a solar array dipole component of 4×10^3 ampere-cm² along the pitch axis. When these numbers are added to those obtained for the S/C-SSU combination, the following (worst case) totals were obtained:

- (1) Roll: $-9.8 \times 10^4 \text{ A-cm}^2$
- (2) Pitch: $-8.2 \times 10^4 \text{ A-cm}^2$
- (3) Yaw: $-9.8 \times 10^4 \text{ A-cm}^2$

In summary, it can be stated that, while the methods just described did not provide the magnetic dipole values with great accuracy, the estimates obtained yielded assurance that magnetic disturbances would be relatively small and would not compromise the success of the mission.

APPENDIX C

SERT II EQUATIONS OF MOTION

It will be convenient for linearization to relate the reference axis system and the body (or principal) axis system in terms of Euler angles. The three sequential rotations required to find the body axes are shown in figure 4. The rotation about Z_r is a yaw angle ψ ; the rotation about y' is a pitch angle θ ; and the rotation about x'' is a roll angle φ . The reference and body systems are related by

$$\begin{bmatrix} x \\ y \\ z \end{bmatrix} = \begin{bmatrix} C\psi C\theta & S\psi C\theta & -S\theta \\ C\psi S\theta S\varphi - S\psi C\varphi & C\psi C\theta + S\theta S\psi S\varphi & C\theta S\varphi \\ C\psi S\theta C\varphi + S\psi S\varphi & S\psi S\theta C\varphi - C\psi S\varphi & C\theta C\varphi \end{bmatrix} \begin{bmatrix} X \\ Y \\ Z \end{bmatrix}_R \quad (C1)$$

The inertial body angular rates can be expressed in terms of Euler angles, Euler angle rates, and the rotation rate of the reference axis system (orbit rate).

$$\omega_x = \dot{\varphi} - \dot{\psi} \sin \theta - \omega_o \sin \psi \cos \theta \quad (C2a)$$

$$\omega_y = \dot{\theta} \cos \varphi + \dot{\psi} \cos \theta \sin \varphi - \omega_o (\cos \psi \cos \varphi + \sin \psi \sin \theta \sin \varphi) \quad (C2b)$$

$$\omega_z = -\dot{\theta} \sin \varphi + \dot{\psi} \cos \theta \cos \varphi - \omega_o (-\cos \psi \sin \varphi + \sin \psi \sin \theta \cos \varphi) \quad (C2c)$$

The satellite dynamics are expressed by Euler's equations of motion:

$$I_{xx} \dot{\omega}_x + \omega_y \omega_z (I_{zz} - I_{yy}) = T_x \quad (C3a)$$

$$I_{yy} \dot{\omega}_y + \omega_x \omega_z (I_{xx} - I_{zz}) = T_y \quad (C3b)$$

$$I_{zz} \dot{\omega}_z + \omega_x \omega_y (I_{yy} - I_{xx}) = T_z \quad (C3c)$$

where I_{jj} is a principal moment of inertia and T_j is an external torque about the j^{th} axis.

Gravity-Gradient Torques (Ref. 9)

Assuming a body in earth orbit is attracted by an inverse-square gravitational force field, the force on a differential mass dm due to the external gravitational field is

$$d\bar{\mathbf{F}} = -\frac{\mu}{r^3} \bar{\mathbf{r}} dm = -\frac{\mu}{r^3} (\bar{\mathbf{r}}_c + \bar{\boldsymbol{\rho}}') dm \quad (\text{C4})$$

where

- μ product of gravitational constant and earth mass
- $\bar{\mathbf{r}}$ radius vector from earth center to dm
- $\bar{\mathbf{r}}_c$ radius vector from earth center to satellite center of mass
- $\bar{\boldsymbol{\rho}}'$ vector locating dm with respect to the center of mass

and $\bar{\mathbf{r}}$, $\bar{\mathbf{r}}_c$, $\bar{\boldsymbol{\rho}}'$ are shown in figure 14.

The differential torque about the center of mass is

$$d\bar{\mathbf{T}}_{gg} = \bar{\boldsymbol{\rho}}' \times d\bar{\mathbf{F}} \quad (\text{C5})$$

and the total gravity-gradient torque is

$$\bar{\mathbf{T}}_{gg} = -\mu \int_m \frac{\bar{\boldsymbol{\rho}} \times (\bar{\mathbf{r}}_c + \bar{\boldsymbol{\rho}}')}{r^3} dm \quad (\text{C6})$$

Since $|\bar{\boldsymbol{\rho}}'| \ll |\bar{\mathbf{r}}_c|$, we can approximate $1/r^3$ by

$$\frac{1}{r^3} = \frac{1}{r_c^3} \left(1 - \frac{3\bar{\mathbf{r}}_c \cdot \bar{\boldsymbol{\rho}}'}{r_c^2} \right) \quad (\text{C7})$$

Now since

$$\bar{\boldsymbol{\rho}}' \times (\bar{\mathbf{r}}_c + \bar{\boldsymbol{\rho}}') = \bar{\boldsymbol{\rho}}' \times \bar{\mathbf{r}}_c$$

equation (C6) becomes

$$\bar{T}_{gg} = -\frac{\mu}{r_c^3} \int_m \left(1 - \frac{3\bar{r}_c \cdot \bar{\rho}'}{r_c^2} \right) (\bar{\rho}' \times \bar{r}_c) dm \quad (C8)$$

From figure 14, we note that in the i, j, k system

$$\bar{\rho}' = x\hat{i} + y\hat{j} + z\hat{k}$$

$$\bar{r}_c = r_c(a\hat{i} + b\hat{j} + c\hat{k})$$

Now, substituting these expressions into equation (C8) gives

$$\bar{T}_{gg} = -\frac{\mu}{r_c^2} \int_m \left[1 - \frac{3(ax + by + cz)}{r_c} \right] [(cy - bz)\hat{i} + (ax - cz)\hat{j} + (bx - ay)\hat{k}] dm \quad (C9)$$

Now choosing i, j, k to be the principal axes of the body, the following relations hold:

$$\int_m x dm = \int_m y dm = \int_m z dm = 0$$

$$\int_m xy dm = \int_m xz dm = \int_m yz dm = 0$$

$$\int_m (y^2 - z^2) dm = I_{zz} - I_{yy}$$

$$\int_m (z^2 - x^2) dm = I_{xx} - I_{zz}$$

$$\int_m (x^2 - y^2) dm = I_{yy} - I_{xx}$$

Thus equation (C9) becomes

$$\overline{T}_{gg} = \frac{3\mu}{r_c^3} \left[bc(I_{zz} - I_{yy})\hat{i} + ac(I_{xx} - I_{zz})\hat{j} + ab(I_{yy} - I_{xx})\hat{k} \right] \quad (C10)$$

Since a , b , c are the direction cosines of r_c in the principal axis system, using equation (C1) and remembering that \overline{r}_c is along the $-Z_R$ axis we find

$$a = \sin \theta$$

$$b = -\cos \theta \sin \varphi$$

$$c = -\cos \theta \cos \varphi$$

and

$$bc = \cos^2 \theta \sin \varphi \cos \varphi$$

$$ac = -\sin \theta \cos \theta \cos \varphi$$

$$ab = -\sin \theta \cos \theta \sin \varphi$$

Thus the gravity-gradient torque may be expressed in terms of Euler angles as

$$\overline{T}_{gg} = \frac{3\mu}{r_c^3} \begin{bmatrix} (I_{zz} - I_{yy})\cos^2 \theta \sin \varphi \cos \varphi \\ -(I_{xx} - I_{zz})\sin \theta \cos \theta \cos \varphi \\ -(I_{yy} - I_{xx})\sin \theta \cos \theta \sin \varphi \end{bmatrix} \quad (C11)$$

For an eccentric orbit, r_c can be expressed as

$$r_c = \frac{a(1 - e^2)}{1 + e \cos \xi}$$

where

e orbit eccentricity

a semimajor axis

ζ true anomaly

For the SERT II orbit, e is small, so the quantity μ/r_c^3 can be approximated as

$$\frac{\mu}{r_c^3} = \omega_o^{*2} \left(1 + 3e \cos \omega_o^* t \right)$$

where

$$\omega_o^* = \sqrt{\frac{\mu}{a^3}}$$

and the time of perigee passage t is equal to 0.

Control Moment Gyros

As shown in figure 5, the CMG reference axes and the body (principal) axes can be related by

$$\begin{bmatrix} \text{ORA}_i \\ \text{SRA}_i \\ \text{IRA}_i \end{bmatrix} = \begin{bmatrix} 0 & 0 & 0 \\ 0 & -\cos \varphi_{gi} & -\sin \varphi_{gi} \\ 0 & \sin \varphi_{gi} & -\cos \varphi_{gi} \end{bmatrix} \begin{bmatrix} x \\ y \\ z \end{bmatrix} \quad (\text{C12})$$

where

$$\varphi_{g1} = +28^\circ \text{ (CMG 1)}$$

$$\varphi_{g2} = -28^\circ \text{ (CMG 2)}$$

Since the CMG's are single-degree-of-freedom gyroscopes, the instantaneous true spin and input axes are related to the CMG reference axes by

$$\begin{bmatrix} OA_i \\ SA_i \\ IA_i \end{bmatrix} = \begin{bmatrix} 1 & 0 & 0 \\ 0 & \cos \sigma_i & \sin \sigma_i \\ 0 & -\sin \sigma_i & \cos \sigma_i \end{bmatrix} \begin{bmatrix} ORA_i \\ SRA_i \\ IRA_i \end{bmatrix} \quad (C13)$$

where σ_i is the CMG gimbal angle of the i^{th} CMG and is positive for a positive rotation about the output axis.

The CMG equations of motion may be expressed as

$$J_i \ddot{\sigma}_i + c_i \dot{\sigma}_i + K_i \sigma_i = \omega_{IAi} h_i + \omega_{Di} h_i + \tau_{TGi} \quad (C14)$$

where

- J_i gimbal inertia of i^{th} CMG
- c_i damping coefficient of i^{th} CMG
- K_i spring constant of i^{th} CMG
- h_i angular momentum of i^{th} CMG
- ω_{IAi} true input axis rate of i^{th} CMG
- ω_{Di} drift rate of i^{th} CMG
- τ_{TGi} programmed torque generator torque of i^{th} CMG

Equation (C14) may be approximated by

$$c_i \dot{\sigma}_i + K_i \sigma_i = \omega_{IAi} h_i + \tau_{TGi} \quad (C15)$$

In equation (C15) we have neglected the CMG inertia and the drift rate. The inertia adds a negligible phase lag to the CMG response, and the drift rate in near zero gravity may be neglected.

Now using equations (C12) and (C13) we can solve (C15) for $\dot{\sigma}_i$:

$$\begin{aligned} \dot{\sigma}_i = & -\frac{K_i \sigma_i}{c_i} + \frac{\tau_{TGi}}{c_i} \\ & + \frac{h_i}{c_i} \left[\omega_y (\cos \varphi_{gi} \sin \sigma_i + \sin \varphi_{gi} \cos \sigma_i) + \omega_z (\sin \varphi_{gi} \sin \sigma_i - \cos \varphi_{gi} \cos \sigma_i) \right] \end{aligned} \quad (C16)$$

Considering the CMG's as sources of external torque on the satellite, the torque on the body from the CMG's may be expressed in the body axis system as

$$\bar{T}_{\text{CMGi}} = -\dot{\bar{h}}_i - \bar{\omega} \times \bar{h}_i \quad (\text{C17})$$

Using equations (C12) and (C13), we find the CMG angular momentum in the body system

$$\bar{h} = h_i \begin{bmatrix} 0 \\ -\cos \varphi_{gi} \cos \sigma_i + \sin \varphi_{gi} \sin \sigma_i \\ -\cos \sigma_i \sin \varphi_{gi} - \sin \sigma_i \cos \varphi_{gi} \end{bmatrix}$$

so

$$-\dot{\bar{h}} = h_i \dot{\sigma}_i \begin{bmatrix} 0 \\ -\cos \varphi_{gi} \sin \sigma_i - \sin \varphi_{gi} \cos \sigma_i \\ -\sin \varphi_{gi} \sin \sigma_i + \cos \varphi_{gi} \cos \sigma_i \end{bmatrix} \quad (\text{C18})$$

and

$$-\omega \times \bar{h} = h_i \begin{bmatrix} \omega_z(-C\varphi_{gi} C\sigma_i + S\varphi_{gi} S\sigma_i) - \omega_y(-C\sigma_i S\varphi_{gi} - S\sigma_i C\varphi_{gi}) \\ \omega_x(-C\sigma_i S\varphi_{gi} - S\sigma_i C\varphi_{gi}) \\ -\omega_x(-C\varphi_{gi} C\sigma_i + S\varphi_{gi} S\sigma_i) \end{bmatrix} \quad (\text{C19})$$

Summing equations (C18) and (C19) gives the CMG torques:

$$\bar{T}_{\text{CMGi}} = h_i \begin{bmatrix} \omega_z(-C\varphi_{gi} C\sigma_i + S\varphi_{gi} S\sigma_i) - \omega_y(-C\sigma_i S\varphi_{gi} - S\sigma_i C\varphi_{gi}) \\ \dot{\sigma}_i(-C\varphi_{gi} S\sigma_i - S\varphi_{gi} C\sigma_i) + \omega_x(-C\sigma_i S\varphi_{gi} - S\sigma_i C\varphi_{gi}) \\ \dot{\sigma}_i(-S\varphi_{gi} S\sigma_i + C\varphi_{gi} C\sigma_i) - \omega_x(-C\varphi_{gi} C\sigma_i + S\varphi_{gi} S\sigma_i) \end{bmatrix} \quad (\text{C20})$$

CMG nonlinearities such as stiction, torquer fade, and drift rate are small (as shown in table II) and may be neglected in this analysis. These nonlinearities are included in the simulations.

Linearized Equations of Motion

The linearized equations of motion are found by assuming that body and CMG angles and rates are small. Equations (C2) may be linearized as follows:

$$\omega_x = \dot{\varphi} - \omega_o \psi \quad (C21a)$$

$$\omega_y = \dot{\theta} - \omega_o \quad (C21b)$$

$$\omega_z = \dot{\psi} + \omega_o \varphi \quad (C21c)$$

where

$$\omega_o = \omega_o^* (1 + 2e \cos \omega_o^* t)$$

Linearizing the derivatives of (C21) gives

$$\dot{\omega}_x = \ddot{\varphi} - \omega_o^* \dot{\psi} \quad (C22a)$$

$$\dot{\omega}_y = \ddot{\theta} - \dot{\omega}_o \quad (C22b)$$

$$\dot{\omega}_z = \ddot{\psi} + \omega_o^* \dot{\varphi} \quad (C22c)$$

where

$$\dot{\omega}_o = -2e \omega_o^{*2} \sin \omega_o^* t$$

Equations (C11) may be linearized for small eccentricity:

$$T_{ggx} = -3(\omega_o^*)^2 (I_{yy} - I_{zz}) \varphi \quad (C23a)$$

$$T_{ggy} = -3(\omega_o^*)^2 (I_{xx} - I_{zz}) \theta \quad (C23b)$$

$$T_{ggz} = -3(\omega_o^*)^2 (I_{yy} - I_{xx}) \theta \varphi \quad (C23c)$$

If it is assumed that $h_1 = h_2 = h$, that $C_1 = C_2 = C$, and that σ_i is small, then using equations (C20), the total linear CMG torques are

$$T_{CMGx} = -h \left[2\dot{\psi} \cos 28^\circ + 2\omega_o^* \varphi \cos 28^\circ + \omega_o^* \cos 28^\circ (\sigma_1 + \sigma_2) \right] \quad (C24a)$$

$$T_{CMGy} = -h(\dot{\sigma}_1 - \dot{\sigma}_2) \sin 28^\circ \quad (C24b)$$

$$T_{CMGz} = h(\dot{\sigma}_1 + \dot{\sigma}_2) \cos 28^\circ + 2h\varphi \cos 28^\circ - 2h\omega_o^* \psi \cos 28^\circ \quad (C24c)$$

Using equations (C16), we find

$$\dot{\sigma}_1 + \dot{\sigma}_2 = -\frac{h}{c} \left[\omega_o^* (\sigma_1 + \sigma_2) \cos 28^\circ + 2\dot{\psi} \cos 28^\circ + 2\omega_o^* \varphi \cos 28^\circ \right] \quad (C25a)$$

$$\dot{\sigma}_1 - \dot{\sigma}_2 = \frac{h}{c} \left[2\dot{\theta} \sin 28^\circ - \omega_o^* (\sigma_1 - \sigma_2) \cos 28^\circ - 4e\omega_o^* \sin 28^\circ \cos \omega_o^* t \right] \quad (C25b)$$

where the torquer torque is

$$\tau_{TGi} = -h\omega_o^* \sin \varphi_{gi}$$

Substituting equations (C21), (C22), (C23), and (C24) into equations (C3) gives

$$\begin{aligned} I_{xx}(\ddot{\varphi} - \omega_o^* \dot{\psi}) + (\dot{\theta} - \omega_o)(\dot{\psi} + \omega_o \varphi)(I_{zz} - I_{yy}) + 3(\omega_o^*)^2(I_{yy} - I_{zz})\varphi \\ + h \left[2\dot{\psi} \cos 28^\circ + 2\omega_o^* \varphi \cos 28^\circ + \omega_o^* (\sigma_1 + \sigma_2) \cos 28^\circ \right] = T_x \end{aligned} \quad (C26a)$$

$$\begin{aligned} I_{yy}(\ddot{\theta} - \dot{\omega}_o) + (\dot{\varphi} - \omega_o \psi)(\dot{\psi} + \omega_o \varphi)(I_{xx} - I_{zz}) + 3(\omega_o^*)^2(I_{xx} - I_{zz})\theta \\ + h(\dot{\sigma}_1 - \dot{\sigma}_2) \sin 28^\circ = T_y \end{aligned} \quad (C26b)$$

$$\begin{aligned} I_{zz}(\ddot{\psi} + \omega_o^* \dot{\varphi}) + (\dot{\varphi} - \omega_o \psi)(\dot{\theta} - \omega_o)(I_{yy} - I_{xx}) + 2h\omega_o^* \psi \cos 28^\circ \\ - h(\dot{\sigma}_1 + \dot{\sigma}_2) \cos 28^\circ - 2h\dot{\varphi} \cos 28^\circ = T_z \end{aligned} \quad (C26c)$$

The second terms of equations (C26a) and (C26c) give rise to the Euler cross-coupling terms. When linearized, the expressions are similar to the gravity-gradient torque terms. Considering the cross-coupling torques as external, the linearized forms are

$$T_x = -(\omega_o^*)^2 \varphi (I_{yy} - I_{zz})$$

$$T_y = 0$$

$$T_z = -(\omega_o^*)^2 \psi (I_{yy} - I_{xx})$$

Equations (C26) may be linearized further and together with equations (C25) completely describe the vehicle motion:

$$I_{xx} \ddot{\varphi} + \varphi \left[4(\omega_o^*)^2 (I_{yy} - I_{zz}) + 2h\omega_o^* \cos 28^\circ \right] + \dot{\psi} \left[\omega_o^* (I_{yy} - I_{xx} - I_{zz}) + 2h \cos 28^\circ \right] + h\omega_o^* (\sigma_1 + \sigma_2) \cos 28^\circ = T_x \quad (C27a)$$

$$I_{yy} \ddot{\theta} + 3(\omega_o^*)^2 (I_{xx} - I_{zz}) \theta + 2e(\omega_o^*)^2 I_{yy} \sin \omega_o^* t + h(\dot{\sigma}_1 - \dot{\sigma}_2) \sin 28^\circ = T_y \quad (C27b)$$

$$I_{zz} \ddot{\psi} + \psi \left[(\omega_o^*)^2 (I_{yy} - I_{xx}) + 2h\omega_o^* \cos 28^\circ \right] + \dot{\varphi} \left[I_{xx} + I_{zz} - I_{yy} \right] \omega_o^* - 2h \cos 28^\circ - h(\dot{\sigma}_1 + \dot{\sigma}_2) \cos 28^\circ = T_z \quad (C27c)$$

$$\dot{\sigma}_1 + \dot{\sigma}_2 = -\frac{h}{c} \left[\omega_o^* (\sigma_1 + \sigma_2) \cos 28^\circ + 2\dot{\psi} \cos 28^\circ + 2\omega_o^* \varphi \cos 28^\circ \right]$$

$$\dot{\sigma}_1 - \dot{\sigma}_2 = \frac{h}{c} \left[2\dot{\theta} \sin 28^\circ - \omega_o^* (\sigma_1 - \sigma_2) \cos 28^\circ - 4e\omega_o^* \sin 28^\circ \cos \omega_o^* t \right]$$

Neglecting initial conditions, the Laplace transformations of equations (C27) can be expressed as

$$\begin{bmatrix} I_{yy}s^2 + 3(\omega_o^*)^2(I_{xx} - I_{yy}) & hs \sin 28^0 \\ -2hs \sin 28^0 & cs + h\omega_o^* \cos 28^0 \end{bmatrix} \begin{bmatrix} \theta(s) \\ \sigma'(s) \end{bmatrix} = \begin{bmatrix} T_y(s) - 2e(\omega_o^*)^2 I_{yy} \frac{\omega_o^*}{s^2 + (\omega_o^*)^2} \\ -4he\omega_o^* \sin 28^0 \frac{s}{s^2 + (\omega_o^*)^2} \end{bmatrix} \quad (C28)$$

and

$$\begin{bmatrix} I_{xx}s^2 + 4\omega_o^*(I_{yy} - I_{zz}) + 2h\omega_o^* \cos 28^0 & s[\omega_o^*(I_{yy} - I_{xx} - I_{zz}) + 2h \cos 28^0] & h\omega_o^* \cos 28^0 \\ s[\omega_o^*(I_{xx} + I_{zz} - I_{yy}) - 2h \cos 28^0] & I_{zz}s^2 + 2h\omega_o^* \cos 28^0 + (\omega_o^*)^2(I_{yy} - I_{xx}) & -hs \cos 28^0 \\ 2h\omega_o^* \cos 28^0 & 2hs \cos 28^0 & cs + h\omega_o^* \cos 28^0 \end{bmatrix} \begin{bmatrix} \varphi(s) \\ \psi(s) \\ \sigma''(s) \end{bmatrix} = \begin{bmatrix} T_x(s) \\ T_z(s) \\ 0 \end{bmatrix} \quad (C29)$$

where

$$\sigma' = \sigma_1 - \sigma_2$$

$$\sigma'' = \sigma_1 + \sigma_2$$

APPENDIX D

SATELLITE SIMULATION

The satellite dynamics were simulated on both analog and digital computers.

Analog

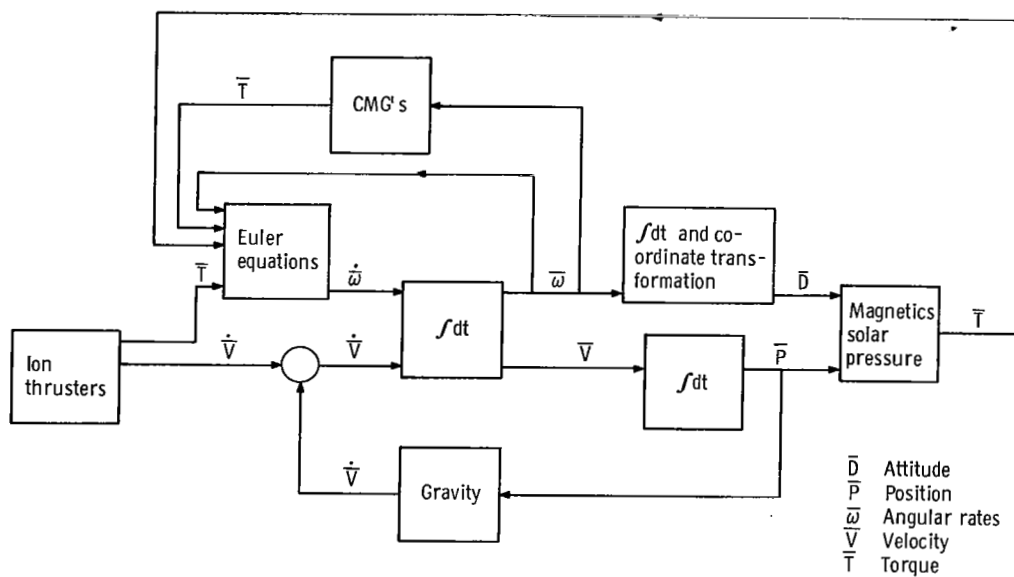
The analog simulation involved rotational dynamics only. Two EAI 231 R-V computers were used for the simulation, which included all torques except magnetic torques. Solar pressure and eccentricity effects could be included without knowledge of the actual spacecraft position.

The analog program was fast and easily adaptable. The studies performed using this program included general stability studies, satellite response to ion thruster operation, and sensitivity to CMG parameters.

Digital

The digital simulation was performed on an IBM 7094-7044 Direct Couple system. The integration scheme was a fourth-order Runge-Kutta method including variable step-size and error control. The simulation included orbit dynamics and was used to study satellite response to magnetic torques. The program was also used to verify analog program results.

Sketch (b) shows a general block diagram applicable to both analog and digital simulations. The digital simulation includes all blocks shown. The analog simulation does not include satellite position simulation or magnetic torques.



APPENDIX E

SYMBOLS

A	area, m^2 (ft^2)
a	semimajor axis, m (ft)
a, b, c	direction cosines of \bar{r}_c
C	cosine
c_i	damping constant of i^{th} CMG, (N)(m)(sec)
e	eccentricity
\bar{F}	force, N (lbf)
\bar{H}	earth magnetic field intensity vector, Oe
H_E	horizontal component of \bar{H} , Oe
h'	length of Agena/spacecraft/spacecraft support unit, m (ft)
h_i	angular momentum of i^{th} CMG, (N)(m)(sec)
I	moment of inertia, $kg-m^2$
IA_i	true input axis of i^{th} CMG
IRA_i	input reference axis of i^{th} CMG
I_{ij}	satellite moments of inertia: $i = x, y, z$; $j = x, y, z$, $kg-m^2$
i	inclination, rad (deg)
J_i	gimbal inertia of i^{th} CMG, $kg-m^2$
K_i	spring constant of i^{th} CMG, N-m/rad
K_w	torsional spring constant, N-m/rad
l_x	component of thruster location along x axis, m
l_z	component of thruster location along z axis, m
m	mass, kg
\hat{n}	unit vector normal to area
OA_i	true output axis of i^{th} CMG
ORA_i	output reference axis of i^{th} CMG
P_s	solar pressure, N/m^2 (lbf/ ft^2)
R	reflectivity

R_E	radius of earth, m
r'	Agena radius, m (ft)
\bar{r}	radius vector from earth center to satellite differential mass dm , m (ft)
\bar{r}_B	moment arm from satellite center of mass to point of force application, m (ft)
\bar{r}_c	radius vector from earth center to satellite center of mass, m (ft)
S	sine
SA_i	true spin axis of i^{th} CMG
SRA_i	true reference spin axis of i^{th} CMG
\hat{s}	unit vector from satellite to sun
T	torque, N-m (ft-lbf)
t	time, sec
α	thruster pitch misalignment, rad (deg)
α'	angle between $-j$ axis and dA in i - j plane, rad (deg)
β	thruster roll misalignment, rad (deg)
β'	instantaneous apparent sun declination referenced to satellite, rad (deg)
γ	phase angle referencing the reference and X'_B, Y'_B, Z'_B axis systems in time, rad (deg)
δ	apparent sun declination in the X'_B, Y'_B, Z'_B axis system, rad (deg)
ξ	true anomaly, rad (deg)
η	angle between earth magnetic dipole axis and radius vector to satellite, rad (deg)
θ	pitch angle, rad (deg)
μ	product of universal gravitation constant and earth mass, m^3/sec^2
$\bar{\rho}$	satellite magnetic moment vector, A-cm ²
$\bar{\rho}_T$	thruster magnetic moment vector, A-cm ²
$\bar{\rho}'$	vector location of differential mass dm with respect to satellite center of mass, m (ft)
σ_i	gimbal angle of i^{th} CMG, rad (deg)
τ_{TGi}	programmed torquer torque of i^{th} CMG, N-m
φ	roll torque

φ_{gi}	mounting angle of i^{th} CMG, rad (deg)
ψ	yaw angle, rad (deg)
Ω	inertial longitude of orbit ascending node, rad (deg)
Ω_E	inertial longitude of Greenwich, rad (deg)
$\bar{\omega}$	inertial body rate vector, rad/sec (deg/sec)
ω_o	instantaneous orbit rate, rad/sec (deg/sec)
ω_o^*	average orbit rate, rad/sec (deg/sec)
ω_{Di}	drift rate of i^{th} CMG, rad/sec (deg/sec)
ω_{IAi}	input axis rate of i^{th} CMG, rad/sec (deg/sec)

Subscripts:

A	aft
ax	axial magnetic component
B	body (principal) axis system
C	coil
CMG	control moment gyro
cc	cross coupling
F	fore
G	geometric axis system
GX, GY, GZ	geometric axis system components
gg	gravity gradient
I	inertial axis system
M	magnetic axis system
max	maximum
norm	normal magnetic component
O	orbit axis system
R	reference axis system
S	sun axis system
ss	steady-state frequency response
step	steady-state step response
T	thruster axis system
x, y, z	body (principal)-axis-system components

REFERENCES

1. Scott, E. D.: Control Moment Gyro Gravity Stabilization. Paper 63-324, AIAA, Aug. 1963.
2. Fischell, Robert E.: Passive Gravity-Gradient Stabilization for Earth Satellites. Torques and Attitude Sensing in Earth Satellites. S. Fred Singer, ed., Academic Press, 1964, pp. 13-30.
3. DeLisle, J. E.; Ogletree, E. G.; and Hildebrant, B. M.: The Application of Gyro-stabilizers to Orbiting Vehicles. Torques and Attitude Sensing in Earth Satellites. S. Fred Singer, ed., Academic Press, 1964, pp. 31-72.
4. Roberson, Robert E.: Generalized Gravity-Gradient Torques. Torques and Attitude Sensing in Earth Satellites. S. Fred Singer, ed., Academic Press, 1964, pp. 73-82.
5. Cake, James E.: A Fortran Code for Computing the Principle Mass Moments of Inertia of Composite Bodies. NASA TM X-1754, 1969.
6. Kendrick, J. B.: TRW Space Data. TRW Systems Group, 1967, p. 76.
7. McElvain, R. J.: Effects of Solar Radiation Pressure upon Satellite Attitude Control. Paper 1918-61, ARS, Aug. 1961.
8. Kraft, J. D.: Guidance and Control. Space Flight Handbooks. Vol. I. Orbital Flight Handbook. Part 3 - Requirements. NASA SP-33, Pt. 3, 1963, pp. XII-40, 41.
9. Greenwood, Donald T.: Principles of Dynamics. Prentice-Hall, Inc., 1965.

TABLE I. - SERT II SPACECRAFT AND ORBIT PARAMETERS

Inertia, kg-m ² :	
Roll, I _{xx}	8.5832×10 ³
Pitch, I _{yy}	10.9451×10 ³
Yaw, I _{zz}	2.7469×10 ³
Spacecraft mass, kg	1.4349×10 ³
Semimajor axis, m	7.378×10 ⁶ (expected)
Eccentricity	0.005 (expected) 0.0003 (measured)
Inclination, deg	99.1 (expected) 99.135 (measured)
Ion thruster thrust, N	2.758×10 ⁻²
Fore thruster location from center of mass, m:	
Along z axis	+2.847
Along x axis	+0.536
Aft thruster location from center of mass, m:	
Along z axis	+2.847
Along x axis	-0.536
Solar array area, m ² (ft ²)	17.65 (190)
Cross-sectional area of Agent (SSU and S/C), m ² (ft ²)	9.01 (97)
Reflectivity of solar array	0.2
Reflectivity of Agena	0.8

TABLE II. - CONTROL-MOMENT-GYRO PARAMETERS

Angular momentum, h, (N)(m)(sec)	4.5
Damping constant, c, (N)(m)(sec)	2.25 to 4.5
Spring constant ^a	0.0
Torquer torque, N-m	2.11×10 ⁻³
Torque fade ^a , N-m/deg	8.7×10 ⁻⁶
Stiction, N-m	1.63×10 ⁻⁵
Drift, N-m	3.25×10 ⁻⁵
Mounting angles (spin reference axes location from negative pitch axis in yaw-pitch plane), ϕ_g , deg	
Gimbal stops, deg from spin reference axes	±28
	±30

^aTorquer fade acts as a very light spring in the CMG. Since spring constant is essentially zero, CMG behaves as rate-integrating gyro with a large angular momentum.

TABLE III. - MAGNETIC DIPOLE MOMENTS

(a) Thrusters

	Torsional pendulum	Field measurements
	Magnetic dipole moment, A-cm ²	
Flight prototype	22.7×10^4	27.7×10^4
Flight thruster 1	-----	27.5
Flight thruster 2	-----	26.6

(b) Spacecraft and spacecraft support unit

	Permanent dipole	Current loop dipole
	Magnetic dipole moment, A-cm ²	
Roll axis	-2.27×10^4	0.10×10^4
Pitch axis	-1.11	.35
Yaw axis	-2.33	.25

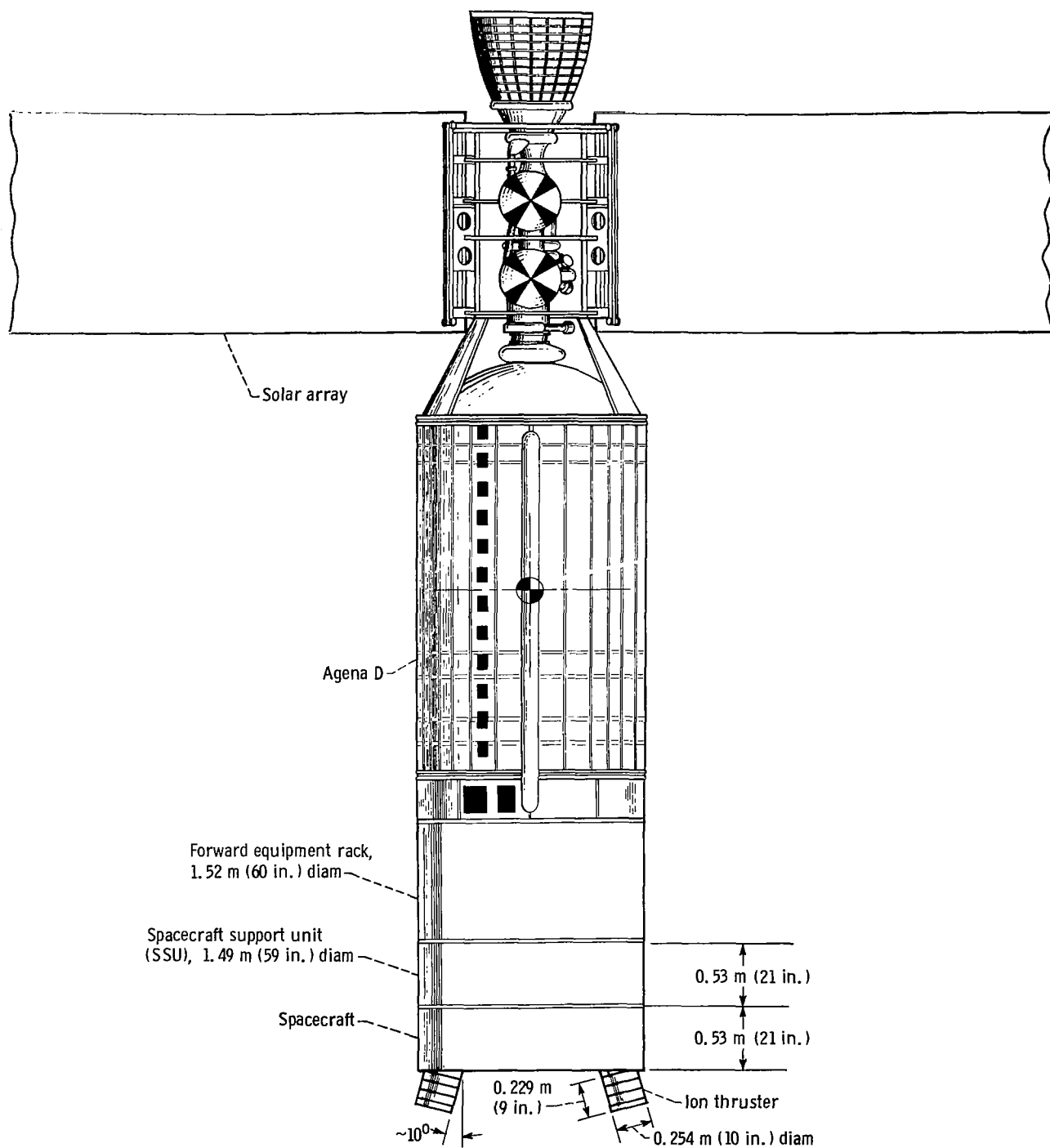
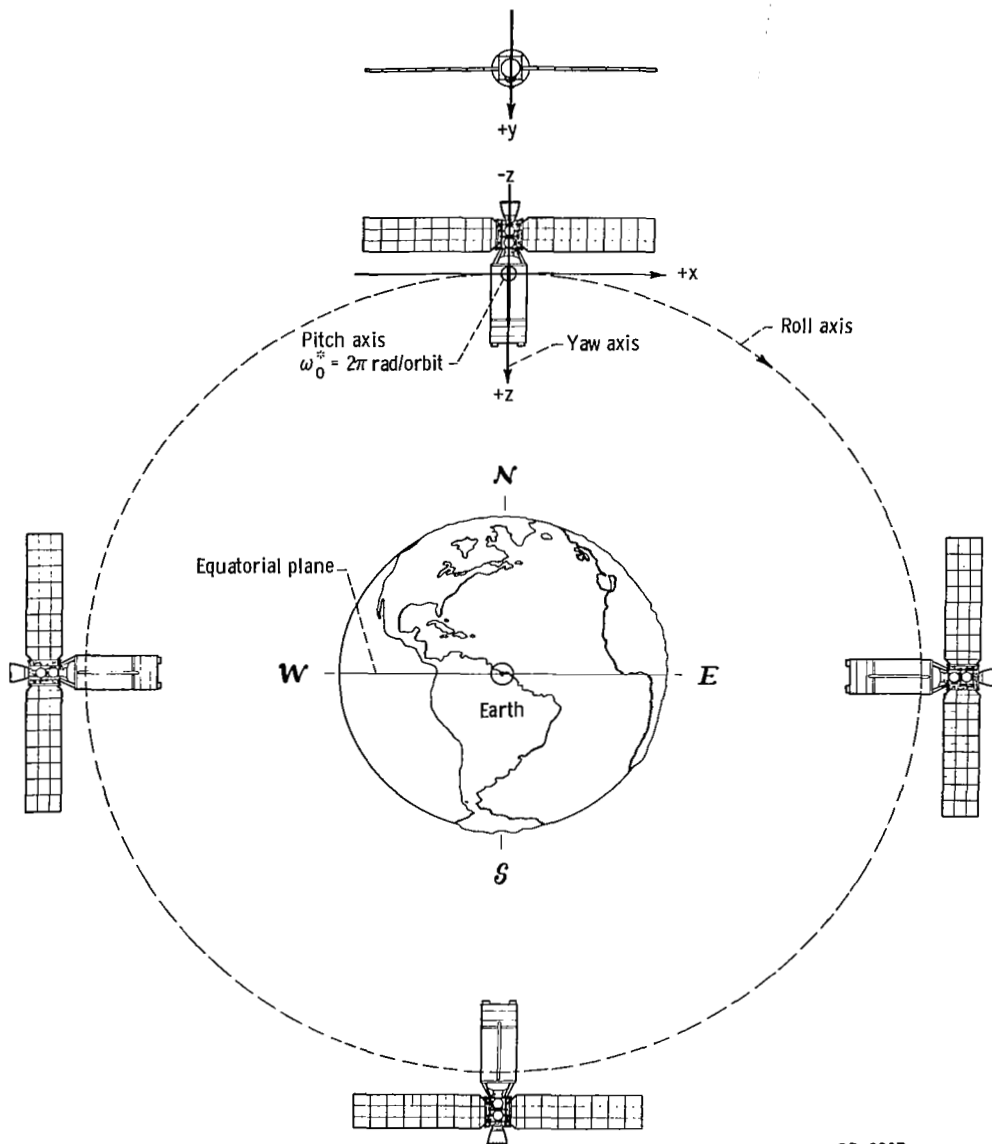


Figure 1. - General arrangement of SERT II spacecraft/Agena D.



CD-9017

Figure 2. - SERT II spacecraft vehicle coordinate system in orbit viewed from sun for spring launch and sunset orbit injection.

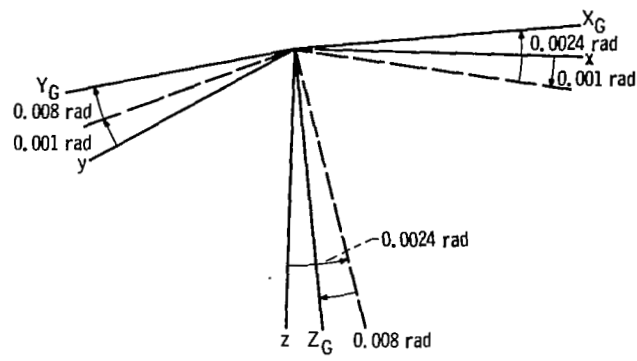


Figure 3. - Body (principal) and geometric axes.

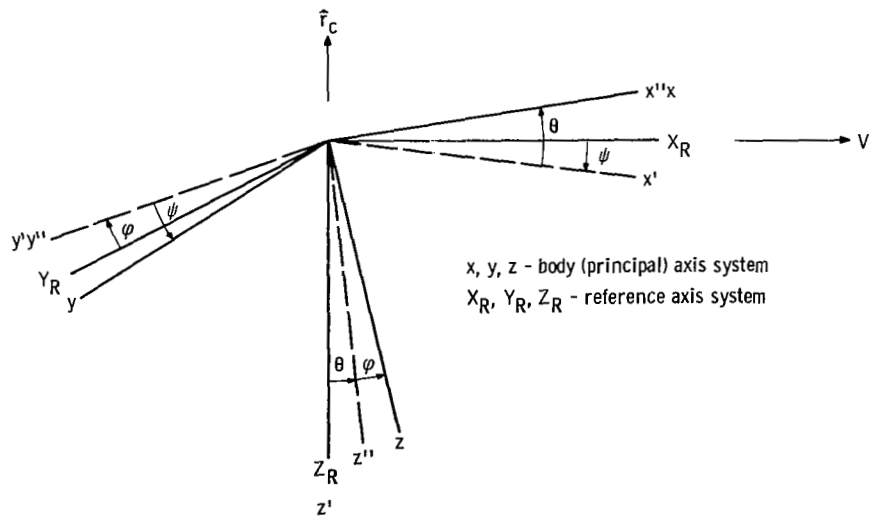


Figure 4. - Reference and body (principal) axis coordinate systems.

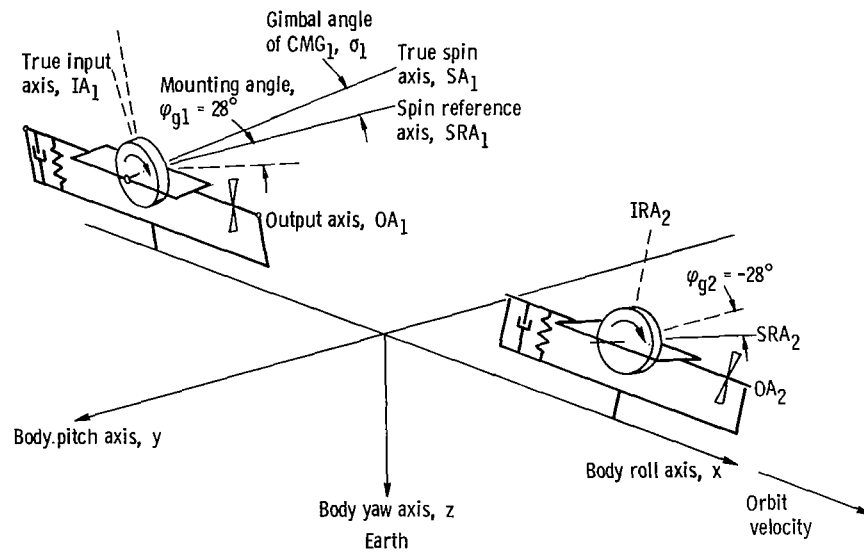


Figure 5. - Control-moment-gyro axes in body axis system. Gimbal stops are located $\pm 30^\circ$ from spin reference axis. Gimbal angle of CMG is a rotation about output axis and is referenced to spin reference axis.

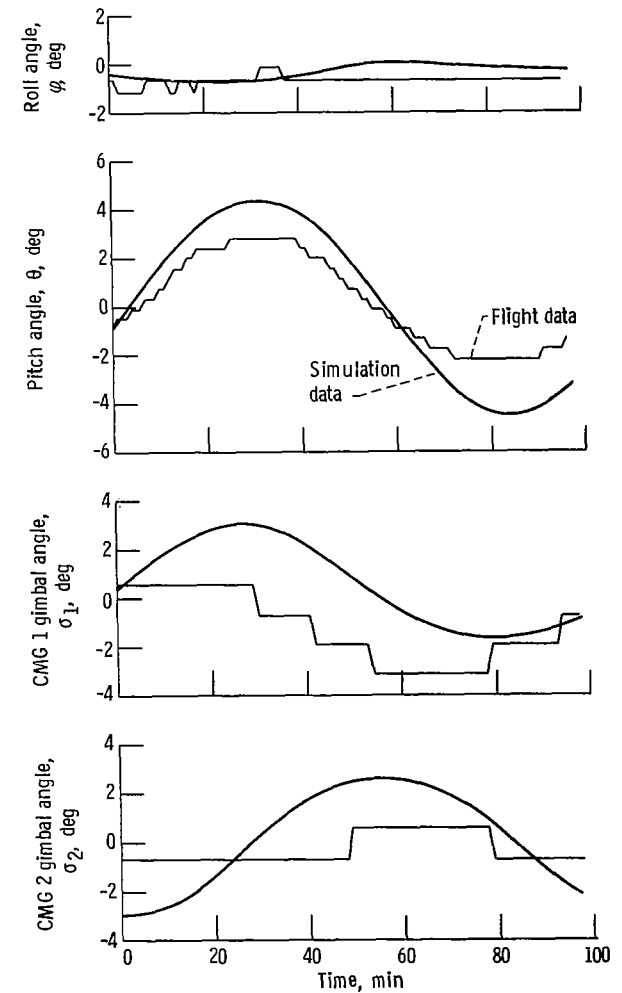


Figure 6. - Worst-case predicted response and flight data.

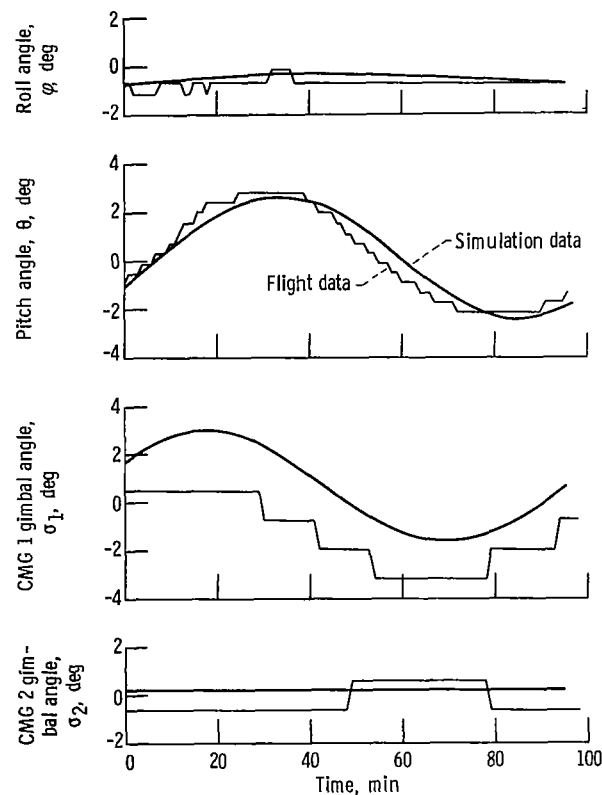
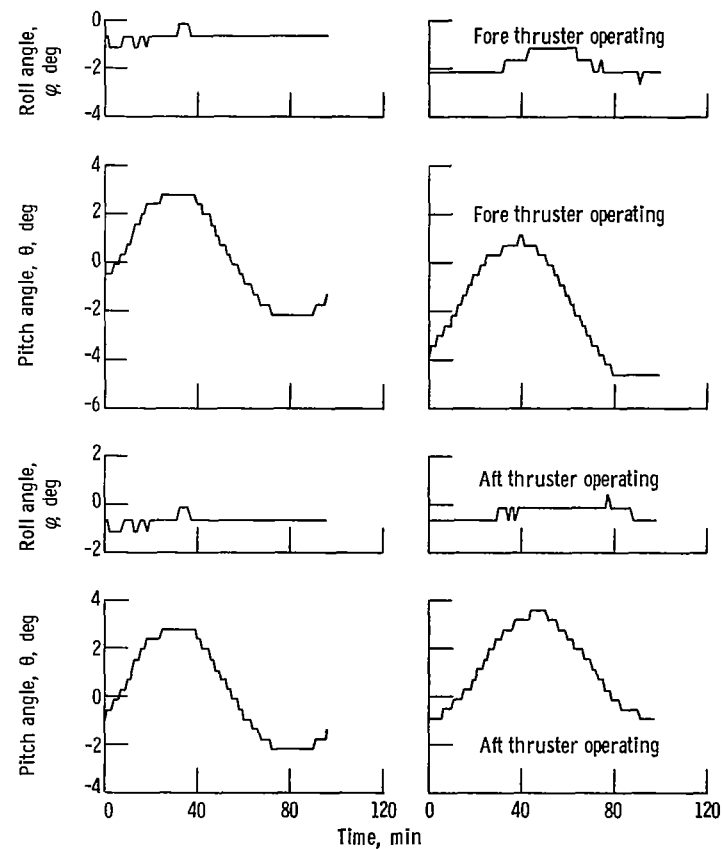


Figure 7. - Flight data and simulated response with estimated magnetic dipole.



(a) Prior to thruster starting - reference data.

(b) Thruster operating.

Figure 8. - Steady-state attitude with thrusters operating.

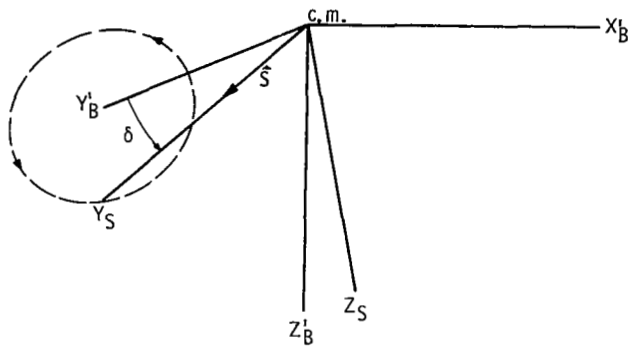


Figure 9. - Apparent sun position.

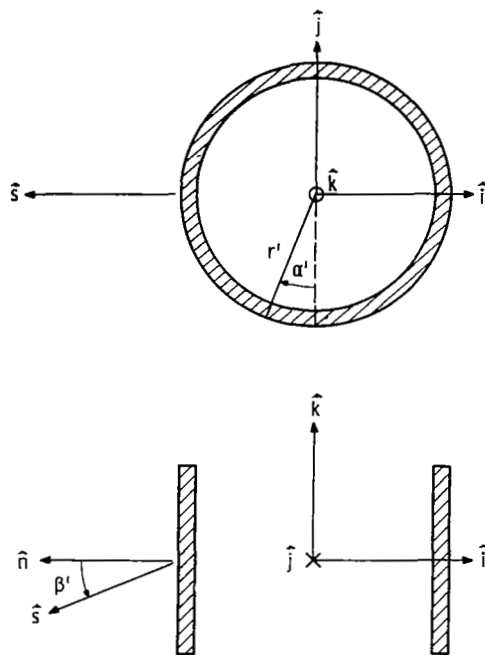


Figure 10. - The \hat{i} , \hat{j} , \hat{k} coordinate system.

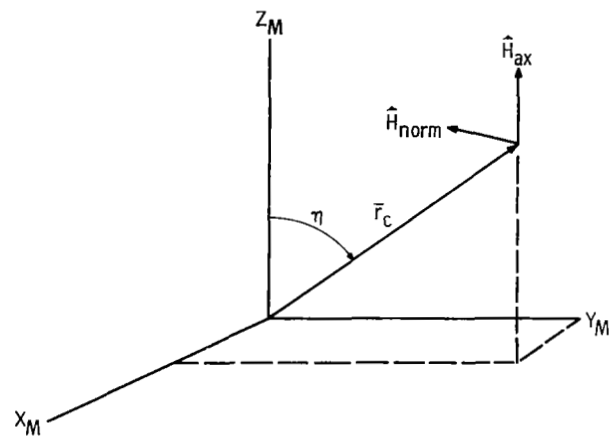


Figure 11. - Unit axial and normal field vectors in the magnetic coordinate system.

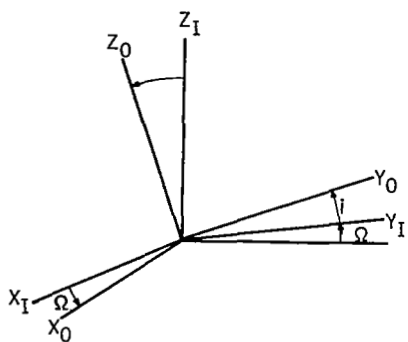
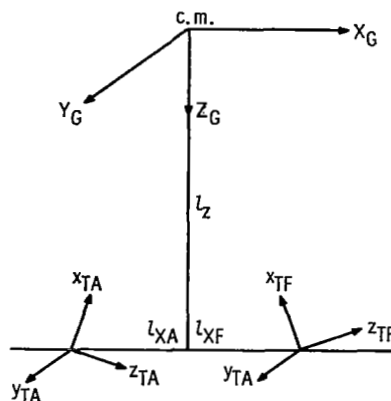
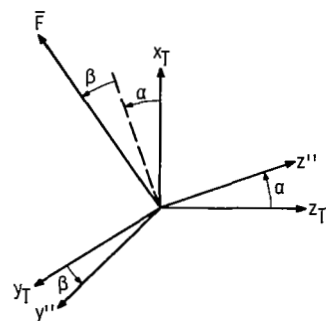
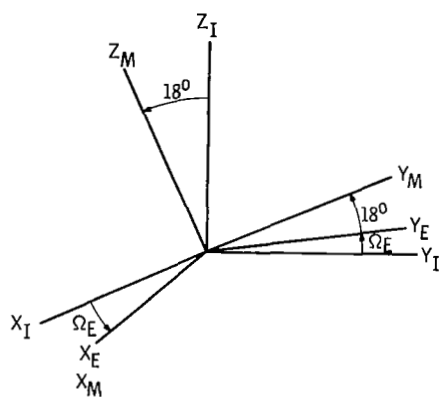


Figure 12. - Inertial, magnetic, and orbit coordinate systems.



A aft thruster
F fore thruster



α rotation about y_T
 β rotation about z''

Figure 13. - Thruster axis systems: x_{TA} and x_{TF} are directed through assumed spacecraft center of mass.

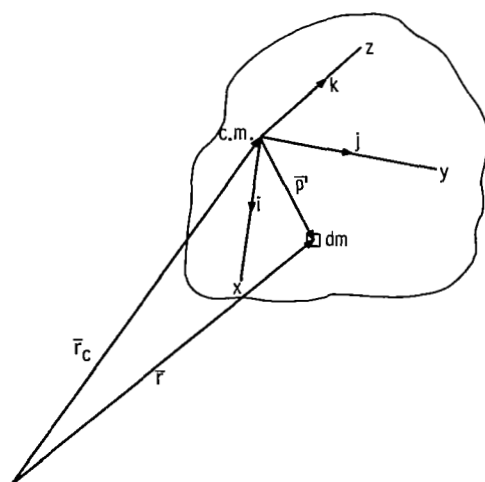


Figure 14. - General body in an inverse-square force field.

NATIONAL AERONAUTICS AND SPACE ADMINISTRATION

WASHINGTON, D. C. 20546

OFFICIAL BUSINESS

PENALTY FOR PRIVATE USE \$300

FIRST CLASS MAIL



POSTAGE AND FEES PAID
NATIONAL AERONAUTICS AND
SPACE ADMINISTRATION

007B 01 C2 UL 31 710723 S00903DS 720401
DEPT OF THE AIR FORCE
WEAPONS LABORATORY /WL0L/
ATTN: E LOU BOWMAN, CHIEF TECH LIBRARY
KIRTLAND AFB NM 87117



POSTMASTER: If Undeliverable (Section 158
Postal Manual) Do Not Return

"The aeronautical and space activities of the United States shall be conducted so as to contribute . . . to the expansion of human knowledge of phenomena in the atmosphere and space. The Administration shall provide for the widest practicable and appropriate dissemination of information concerning its activities and the results thereof."

— NATIONAL AERONAUTICS AND SPACE ACT OF 1958

NASA SCIENTIFIC AND TECHNICAL PUBLICATIONS

TECHNICAL REPORTS: Scientific and technical information considered important, complete, and a lasting contribution to existing knowledge.

TECHNICAL NOTES: Information less broad in scope but nevertheless of importance as a contribution to existing knowledge.

TECHNICAL MEMORANDUMS: Information receiving limited distribution because of preliminary data, security classification, or other reasons.

CONTRACTOR REPORTS: Scientific and technical information generated under a NASA contract or grant and considered an important contribution to existing knowledge.

TECHNICAL TRANSLATIONS: Information published in a foreign language considered to merit NASA distribution in English.

SPECIAL PUBLICATIONS: Information derived from or of value to NASA activities. Publications include conference proceedings, monographs, data compilations, handbooks, sourcebooks, and special bibliographies.

TECHNOLOGY UTILIZATION PUBLICATIONS: Information on technology used by NASA that may be of particular interest in commercial and other non-aerospace applications. Publications include Tech Briefs, Technology Utilization Reports and Technology Surveys.

Details on the availability of these publications may be obtained from:

SCIENTIFIC AND TECHNICAL INFORMATION OFFICE

NATIONAL AERONAUTICS AND SPACE ADMINISTRATION

Washington, D.C. 20546